# DETERMINATION OF URANIUM CONCENTRATION IN WATER BY MICROSAMPLE X-RAY ANALYSIS (MXA)

By

NORIKO SHIBUYA

A THESIS PRESENTED TO THE GRADUATE SCHOOL
OF THE UNIVERSITY OF FLORIDA IN PARTIAL FULFILLMENT
OF THE REQUIREMENTS FOR THE DEGREE OF
MASTER OF SCIENCE

UNIVERSITY OF FLORIDA

2003

To my family

ACKNOWLEDGMENTS

I thank Dr. Ronald Baney, my advisor and the supervisory committee chair, for his support. Without his constant encouragement, I could not have completed this work. I also thank Prof. James Tulenko for his guidance and dedication to provide the best possible working condition for the students. I would also like to extend my gratitude to Dr. E. Dow Whitney and Dr. Darryl Butt, for their help and patience.

This work was funded through a grant Nuclear Engineering Research Initiative (NERI) project #99-0153 Advanced Proliferation Resistant, Lower Cost Uranium-Thorium Dioxide Fuels for Light Water Reactors.

TABLE OF CONTENTS

LIST OF TABLES

LIST OF FIGURES

Abstract of Thesis Presented to the Graduate School
of the University of Florida in Partial Fulfillment of the
Requirements for the Degree of Master of Science

DETERMINATION OF URANIUM CONCENTRATION IN WATER
BY MICROSAMPLE X-RAY ANALYSIS (MXA)
By

Noriko Shibuya

August 2003

Chair: Ronald H. Baney
Major Department: Materials Science and Engineering

The need for environmental monitoring is higher than ever, as the public becomes more aware of the environmental issues--one of them being the potential contamination of the groundwater in the vicinity of the spent nuclear fuel repository site. There is a concern with regard to the stability of the spent $UO_2$ fuel in a long-term storage condition. If not properly stored, uranium can leach out of the matrix, and may eventually contaminate the surroundings. To improve on the stability of the spent fuel in storage, the use of mixed oxide fuel (U, Th)$O_2$ (urania-thoria) was considered. To provide proof to the hypothesis that thorium aids in suppressing uranium from leaching out of the matrix, dissolution experiments of the urania-thoria pellets were carried out. Pellets of different uranium content were immersed in J-13 ground water (well water obtained at Yucca Mountain), and the concentration of U(VI) in the water was monitored at different time intervals. It is this experiment that called for a new technique for the determination of uranium concentration in water in a rapid, inexpensive, and simple manner.

As part of this study, a microsample X-ray analysis (MXA) sample preparation technique for U detection in water samples was developed. The development of this sample preparation technique constitutes the subject of this thesis. The MXA method uses a 50-μL aliquot of liquid specimen for one sample preparation. A droplet of the analyte solution was loaded onto a sample cup with an X-ray window film and allowed to dry completely. The dry residue from the analyte was measured by the Energy Dispersive X-ray Fluorescence (EDXRF) Spectrometer. In this study, polyester film was used as the X-ray window for all samples.

A 1000-ppm U(VI) solution was diluted with nanopure water in appropriate proportions for a calibration curve construction. Samples (concentration range: 0 to 500 ppm) were also made from the 1000-ppm U solution, and were measured based on the calibration curve. The results were compared to the known concentrations. The same samples were measured on a uranium analyzer for comparison. Error analysis was performed to identify the possible sources of error. Results obtained from the samples prepared by the MXA method and measured on the EDXRF (MXA-EDXRF) were in good agreement with those of the uranium analyzer. An MXA-EDXRF sample, on the average, has the error size of less than 15%, which makes the MXA-EDXRF technique a rapid, simple, and accurate method for determining the uranium concentration in water down to the 1-ppm level.

# CHAPTER 1
# INTRODUCTION

## Motivation

Ever since the issue of environmental protection was raised, there is a continuing demand for environmental monitoring. The pollutants from various sources gradually accumulate at many levels within the ecosystem, and their effect on the ecosystem can be devastating in a long run. Thus, over the years, numerous instruments and methods have been developed and adopted for environmental analysis.[1-6] Environmental samples can be in various forms. So, it is desirable that the analytical instruments and the sample preparation methods be flexible and able to handle highly diverse samples. One example of such an instrument is the X-ray Fluorescence (XRF) Spectrometer. XRF is a characterization instrument used to identify and quantify the amount of elements, which are present in a wide range of samples: gases, solids, or liquids. XRF uses X-rays to cause characteristic fluorescence emission from the specimen atoms. Those characteristic signals are detected to identify which elements are present, and their relative intensities can be used to quantify the amounts of those elements.

In this study, of numerous environmental issues, a focus was given to the monitoring of trace U levels in ground water in the vicinity of a geological repository for spent nuclear fuels. The leaching of radionuclides from spent $UO_2$ fuel during a long-term geological storage is a major concern. The leaching of uranium and other hazardous radionuclides might eventually lead to the contamination of the groundwater in the repository area. Thus, ways to stabilize the spent $UO_2$ were investigated. Utilization of

the mixed oxide fuel (U, Th)$O_2$ (urania-thoria) in place of $UO_2$ was considered as a possible solution for the leaching of radionuclides.[7] In addition to the material stabilization, the use of urania-thoria has two more advantages: thorium is abundant, and offers better proliferation-resistance. Therefore, the effect of thorium on the leaching behavior of mixed oxide fuel was investigated.[7] If thoria proves to be able to stabilize the spent fuel matrix during the long term geological storage, then urania-thoria will be considered superior to $UO_2$ as a waste form.

Urania-thoria can form a solid solution, since both U and Th can exist in the +4 oxidation state. $ThO_2$ (thoria) is a stable and insoluble oxide. The highest oxidation state for Th is Th(IV), while U(IV) can undergo further oxidation (up to U(VI)). Under some conditions, U(IV) may oxidize within the urania-thoria matrix, creating a heterogeneous, oxygen-rich portions. Since U(VI) species are able to form more soluble phases, the oxygen-rich regions in the urania-thoria matrix would be prone to leaching of radionuclides.[7]

The objective of the Nuclear Engineering Research Initiative (NERI) project #99-0153 Advanced Proliferation Resistant, Lower Cost Uranium-Thorium Dioxide Fuels for Light Water Reactors[7] was to determine and quantify the thorium stabilization ability in urania-thoria as a function of the composition. Urania-thoria pellets, with compositions of 5, 23.6, 36.8, 50, and 100 mol-% U, were fabricated by blending, pressing, and sintering $UO_2$ and $ThO_2$ powders. The pellets were placed in flasks containing J-13 ground water[7] (supplied by the Office of Civilian Waste Management at Yucca Mountain) to observe their dissolution behavior under inert gas atmosphere. It was expected that the higher the thoria content is, the lower the leaching rate. To keep track of the leaching behavior, the

concentration of U(VI) in the J-13 leachant water was measured at various time intervals. It was for this step that a U(VI) detection method in water samples was needed.

It is desirable to have more characterization methods available, so that one will be able to choose methods based on: availability of resources, cost, accuracy, and simplicity. The objective was to find a U detection method for water samples that is effective, inexpensive, and has a large sample handling capacity. This study is a compilation of the development of this new [U(VI)] detection method, which is inexpensive, simple, and rapid. The effectiveness of the new method of measuring [U(VI)] was verified by comparing the results to that of uranium analyzer UA-3 manufactured by Scintrex (Denton, TX) . Since the XRF is an X-ray instrument, some basics on the theory behind X-rays and XRF will be presented first.

## X-Ray Properties

Since its discovery in 1895 by W. Röntgen,[1] X-rays have been utilized in numerous areas. X-rays, which are a form of electromagnetic radiation with a short wavelength, play an important role in medical, industrial, and other scientific fields. One significant use of X-rays is materials characterization. There are a number of different characterization techniques that use X-rays. Among those are X-Ray Diffraction (XRD), which is predominantly used to study the crystalline state of materials, and XRF, which can take samples in a variety of forms. XRF measures the characteristic radiation, given off by different materials when irradiated by X-ray beams, for elemental analysis. A few basic concepts concerning X-ray are given in the following.

The origin of X-rays lies in a series of events involving atomic electrons. Upon irradiation, an electron is excited to a higher energy state, followed by a transition of the excited electron from high- to low-energy state. The second step, during which the

electrons are restored to their original, low-energy state, is accompanied by X-ray photon production. When a substance is irradiated by monochromatic X-ray photons, three phenomena occur: scattering, absorption, and fluorescence. A brief discussion on each of them is given below.

**Scattering and Absorption**

Coherent (no energy loss) scattering can lead to more interference, which generates diffraction maxima. The angles at which diffraction maxima occur are related to the plane spacing in a crystal structure of materials. This property is used to investigate the structure of materials, which led to the development of the XRD technique.

Absorption, along with the scattering, is one of the processes in which X-rays traveling inside a material are attenuated. A majority of attenuation occurs via photoelectric absorption. The fraction of the incident X-ray that is attenuated inside matter increases with the atomic number of the matter. Thus, the fraction of X-ray traveling out of matter is related to the average atomic number of the material irradiated by the incident X-ray. The average atomic number distribution across a material is also related to the distribution of the X-ray intensity coming out of the material. It is this principle upon which the X-ray imaging (radiograph) is based. The following expression describes the relationship between the incident and the transmitted beam:

$$I(\lambda) = I_0(\lambda)\exp(\mu\rho x) \tag{1-1}$$

in which $I$ is the transmitted beam intensity, $I_0$ is the incident beam intensity, $\mu$ is the mass attenuation coefficient of the specimen through which the beam is transmitted, $\rho$ is the density of the specimen, and the x is the distance traveled by the beam through the specimen.[2]

**Electron Configurations**

To understand the mechanism of characteristic radiation emission, some basic knowledge on the electron configuration is essential, as allowed and forbidden electron transitions are characterized by the quantum numbers. The quantum numbers, by definition, describe the amount of energy associated with electrons.[1, 2]

Table 1-1. Summary of quantum numbers

| Quantum number | Possible values |
|---|---|
| Principal, *n* | 1, 2, 3, 4, … |
| Angular, *l* | 0, 1, 2, 3, …, (*n*-1) |
| Magnetic, *m* | 0, ±1, ±2, …, ±*l* |
| Spin, *s* | ±1/2 |

The Pauli exclusion principle states that no two electrons in an atom can have the exact same set of quantum numbers. The following table describes the atomic structure by quantum numbers.[1]

Table 1-2. Atomic structures of *K*, *L*, and *M* shells

| Shell; e- | *n* | *l* | *m* | *s* | Orbitals |
|---|---|---|---|---|---|
| *K* (2) | 1 | 0 | 0 | ±1/2 | 1*s* |
| *L* (8) | 2 | 0 | 0 | ±1/2 | 2*s* |
| | 2 | 1 | 1 | ±1/2 | |
| | 2 | 1 | 0 | ±1/2 | 2*p* |
| | 2 | 1 | -1 | ±1/2 | |
| *M* (18) | 3 | 0 | 0 | ±1/2 | 3*s* |
| | 3 | 1 | 1 | ±1/2 | |
| | 3 | 1 | 1 | ±1/2 | 3*p* |
| | 3 | 1 | -1 | ±1/2 | |
| | 3 | 2 | 2 | ±1/2 | |
| | 3 | 2 | 1 | ±1/2 | |
| | 3 | 2 | 0 | ±1/2 | 3*d* |
| | 3 | 2 | -1 | ±1/2 | |
| | 3 | 2 | -2 | ±1/2 | |

Figure 1-1 illustrates the deexcitation schemes in which different kinds of characteristic emission occur. The first letter (K, L, M, *etc*.) refers to the destination of electrons (or where the vacancy was in the beginning). The second letter (Greek letter) tells where the electron is coming from to fill the vacancy.

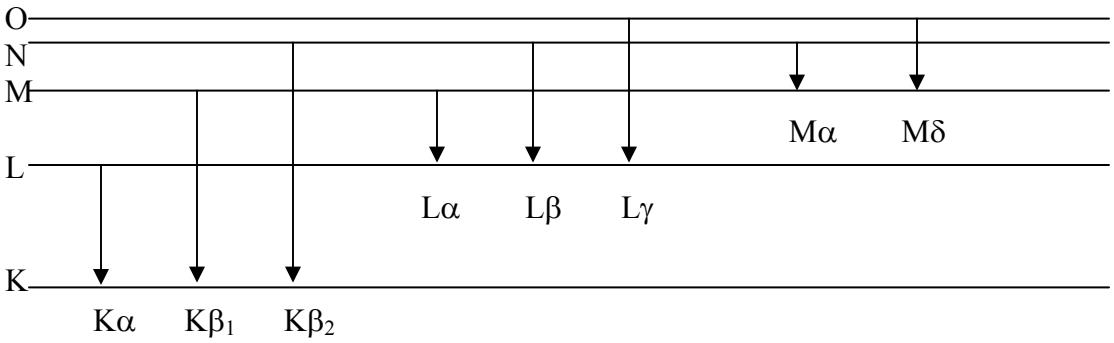


Figure 1-1. Deexcitation schemes (X-ray series)

The emissions are characteristic, because: 1) the energies correspond with the energy difference of the initial and the final energy states of each emission, and 2) quantum energies are characteristic of elements from which the emissions arise.

In the following, explanations on how the characteristic emissions are utilized for X-ray Spectrometry are given.

**X-Ray Spectrometry**

Secondary radiation, produced by matter when hit by an X-ray, is characteristic for each element making up a specimen. The X-ray spectrometry technique uses this feature for materials characterization, namely chemical composition analysis. The secondary radiation from the specimen is detected, and the characteristic wavelength for individual component is determined. Intensities of the isolated components can be used to calculate the elemental concentrations with proper sample preparation procedure and calculation method.

There are two ways to isolate the narrow energy bands for wavelength calculation. One way is to use a single crystal to diffract the polychromatic beam given off by the specimen. This method is utilized in Wavelength Dispersive Spectrometry (WDS). Alternative way is to use a proportional detector in the same setup. This method is called Energy Dispersive Spectrometry (EDS) (a brief comparison of the two will be discussed later). General principles of how WDS and EDS work, and more details of characteristic emissions can be found below.

**Continuum Radiation (Bremsstrahlung)**

As a result of a high-energy electron beam hitting the surface of a specimen, several kinds of beams will emerge. One of them is called continuum radiation, which refers to a radiation emission that spans a wide, continuous range of wavelength. Also referred to as white radiation or bremsstrahlung, the continuum radiation is a direct result of electrons in the incident beam decelerated by atomic electrons in the specimen. The minimum detectable wavelength depends on the operating voltage.[2] The following expression approximates the minimum detectable wavelength[1, 2]

$$\lambda_{\min} = \frac{12.4}{V} \tag{1-2}$$

in which $\lambda_{min}$ is in Å, and $V$ is the operating voltage in kV. The higher the voltage of the incident beam (operating voltage), the shorter the minimum detectable wavelength will be. However, as the operating voltage increases, the actual minimum wavelength corresponding to the voltage will be slightly larger than that predicted by Equation 1-2. This is due to incoherent (Compton) scattering, in which X-ray photons interact with atomic electrons in the specimen and lose some of their energy as a result. This is likely

to occur, when the X-ray photon collides with an outer electron in target elements that are loosely bound. The electron is drawn back as it collides with an X-ray photon, taking away a small amount of energy from the incident X-ray photon. The X-ray photons will be deflected with a smaller energy than before, which results in a longer wavelength. The relationship between the incident wavelength $\lambda_0$ and the scattered wavelength $\lambda_C$ is as follows:

$$\lambda_C - \lambda_0 = 0.0242(1 - \cos\psi) \tag{1-3}$$

in which $\psi$ is the angle over which the X-ray beam is scattered.[1] Since most of the commercial spectrometers have $\psi$ equal to 90°, the difference between the coherently and incoherently scattered beams is around 0.0242 Å.

The continuum radiation has an intensity profile as follows: the intensity starts at zero at $\lambda_{min}$, then increases to reach its maximum around 1.5 to 2 times the $\lambda_{min}$, and then gradually decreases as the wavelength increases.[2] As the operating voltage increases, the maximum of the continuum shifts towards the shorter wavelength region. For example, characteristic lines of molybdenum Mo $K_\alpha$ ($\lambda$=0.71 Å) and Mo $K_\beta$ ($\lambda$=0.63 Å) appear only when the operation potential is increased above 20 kV.[1]

Most commercial models of spectrometer have an X-ray tube, an excitation source, in which a heated tungsten filament is used as an electron source. A layer of pure metals (chromium, rhodium, tungsten, *etc.*) is employed as the anode. The anode material with a higher atomic number is capable of producing more intense beams. If target elements have low atomic numbers, however, anode materials with higher atomic number may not be suitable. This is due to the fact that high atomic number anode materials require a

thicker exit window in the tube (a thicker exit window absorb low-energy beams, especially of low atomic number elements).

The focus of the discussion now will be shifted to the resulting characteristic radiation from the incident X-ray beam generation.

**Characteristic Radiation**

When a particle, such as an electron, collides with a bound electron in a target atom, the bound electron can be ejected, provided that the incident particle had energy greater than the binding energy of the atomic electron. The ejected atomic electron is called a photoelectron, and the whole process is termed the photoelectric effect. If the electron shell has vacancies, the atom is unstable (it is not in its lowest energy state). Thus, it is energetically favorable for the atom to undergo a process in which it achieves stability (its lowest energy state). There are two processes that may take place to achieve that. The first process, the Auger effect, does not result in X-ray photon emission from the atom in question. Another photoelectron (called Auger electron) is emitted from the atom instead. The discovery of this effect had lead to the development of another characterization method, Auger electron spectroscopy (AES). In the second process, the excited atom can be stabilized when one of its outer electrons moves to fill the vacancy. This process causes an emission of an X-ray photon, whose energy is equal to the difference of the initial and the final energies of the electron filling the vacancy. All X-ray photons emitted this way have energies proportional to the energy state differences of atomic electrons, so the lines from the emitted X-ray photons will be characteristic of each element. H. G. Moseley first described the relationship between the wavelength $\lambda$ of the X-ray photon and the atomic number Z of the excited atom as Moseley's law:[1,2]

$$\frac{1}{\lambda} = K\left[Z - \sigma\right]^2 \tag{1-4}$$

in which $K$ is a constant that depends on each spectral series, $\sigma$ is the shielding constant (slightly less than unity).[1, 2] The wavelength of the X-ray photon is given by

$$\lambda = \frac{12.4}{E} \tag{1-5}$$

in which $E$ is the energy of the photon.[1, 2] An atom can give off several different X-ray wavelengths, depending on the paths that an electron takes.

To illustrate how electrons transfer, some rules involving quantum numbers apply. First, the principal quantum number $n$ and the angular quantum number $l$ should change by 1, and the vector sum of $(l + s)$ should be a number and it should change by 1 or 0, where $s$ is the spin quantum number with a value ±1/2. For $K$ and $L$ series (vacancies in $K$ level give rise to $K$ series and likewise for $L$ series, where $K$ and $L$ refer to the electron shells), the allowed transitions are summarized in the following table.

Table 1-3. Allowed electron transition in $K$ and $L$ shells

| ***K* series** | ***L* series** |
|---|---|
| $p \rightarrow s$ | $p \rightarrow s$, $s \rightarrow p$, $d \rightarrow p$ |

As mentioned earlier, the Auger effect and the production of characteristic X-ray photons are in competition. Which of these are preferred depends on the atomic number of the target element. The fluorescence yield, or the number of quanta of $K$ series radiation arising from one atom, is fixed for each atomic number. In general, the fluorescence yield for $K$-series drops rapidly below the atomic number around 40, and eventually drops to zero below the atomic number around 10. This is the reason that X-ray fluorescence is extremely difficult to apply to low-atomic number elements. On the other hand, the fluorescence yield of $K$-series electrons increases above the atomic number 40, and plateaus at slightly less than unity above the atomic number of 80 and

beyond.[1] Therefore, the higher the atomic number, the more likely the fluorescence to occur, while the lower the atomic number, the Auger effect dominates. In general, X-ray fluorescence spectroscopy is preferred for higher-atomic number elements, and Auger electron spectroscopy is chosen for lower-atomic number elements. The figure below summarizes how the X-ray photons interact with a specimen.

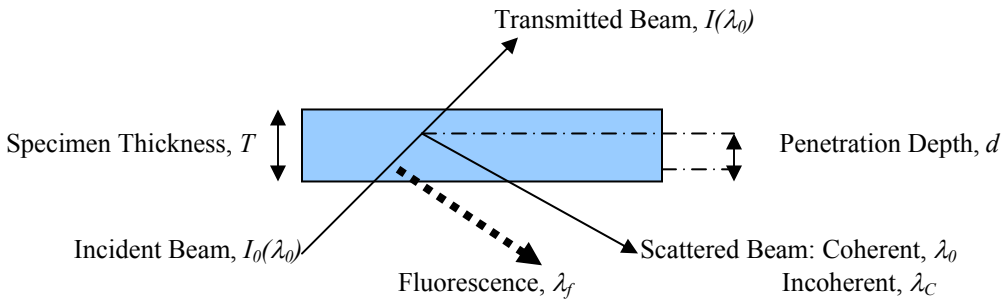


Figure 1-2. Interaction of the incident X-ray beam with the specimen

As mentioned earlier, the XRF technique, which utilizes the fluorescence as a means to characterize materials, has two types of instruments: EDXRF and WDXRF. They will be compared in the following section.

## X-Ray Fluorescence Spectrometry

### Two types of XRF

There are two kinds of equipments in the X-ray fluorescence spectrometry: the energy dispersive X-ray fluorescence (EDXRF) spectrometer, which became commercially available in the early 1970s, and the wavelength dispersive X-ray fluorescence (WDXRF) spectrometer, which came into existence in the early 1950s. The choice between the two categories of XRF for particular analyses depends on which aspects of the analyses can be compromised. For a rapid, quantitative analysis, a simultaneous WDXRF is a good choice, provided a high initial cost is justified. To cover a wide variety of specimens in a relatively short time, a sequential WDXRF is suitable,

again for a high initial cost. If the initial cost is the biggest issue, and the detection limits and/or accuracy can be compromised to a certain degree, or the analysis can be qualitative or semiquantitative, an EDXRF is a reasonable choice.[6] There are four major differences between the EDXRF and WDXRF: 1) the X-ray excitation source, 2) the price range, 3) the number of elements that can be measured at a time, and 4) the data collection time.

In general, all XRF systems are controlled by personal computers, and are capable of measurements of Z = 11 (sodium) and higher. All are sensitive enough for measuring samples down to low parts per million (ppm) or tenths of a percent range. Some of the differences between the WDXRF and EDXRF are reviewed in the following sections.

**Range of Measurable Elements**

The range of elements on the periodic table that can be measured is different. The absolute sensitivity of both techniques decreases dramatically as the atomic number of the target element decreases. This decrease is caused by the reduction in the fluorescence yield in the low atomic number region and the decrease in the bremsstrahlung X-ray photons with long wavelength, which are influenced by the X-ray tube design and the X-ray excitation source. Another reason for the decreased sensitivity is due to the dominance of the absorption effect in the long wavelength region, which is influenced by the instrument design and the detector. EDXRF typically employs the Si(Li) diode detector. The Si(Li) detector has a contact layer on the surface, which is comprised of about 0.02 μm thick film of gold and a 0.1 μm thick dead silicon layer. It is the thickness of this layer that causes the low-energy, long wavelength X-ray photons to be absorbed (in the dead silicon layer) at a high probability. However, development of thinner

windows for the Si(Li) detector made it possible to bring down the lowest atomic number element measurable to about Z = 8 (oxygen) for the top-of the-line EDXRF systems. Conventionally, the low atomic number limit for WDXRF is Z = 9 (fluorine). On a specially-setup WDXRF system, the limit can go down to about Z = 4 (beryllium).

**Resolution**

Resolution is the ability of the system to distinguish the characteristic lines that are close to one another (usually expressed in eV, which refers to the energy difference between adjacent lines). The difference in the detector design is primarily responsible for the resolution difference for EDXRF and WDXRF. For WDXRF, dispersion by the analyzing crystal (LiF(200), for example) and the allowed divergence of the collimator influences the resolution of a system. EDXRF utilizes a Si(Li) detector that takes a distribution of voltage pulses proportional to the signal intensity, and a multichannel analyzer isolates the voltage pulses to discrete units (the consecutive output of these discrete units makes a complete spectrum). In general, typical resolution for the WDXRF ranges from 10 to 100 eV, while that of EDXRF system is about 150 to 250 eV.[3]

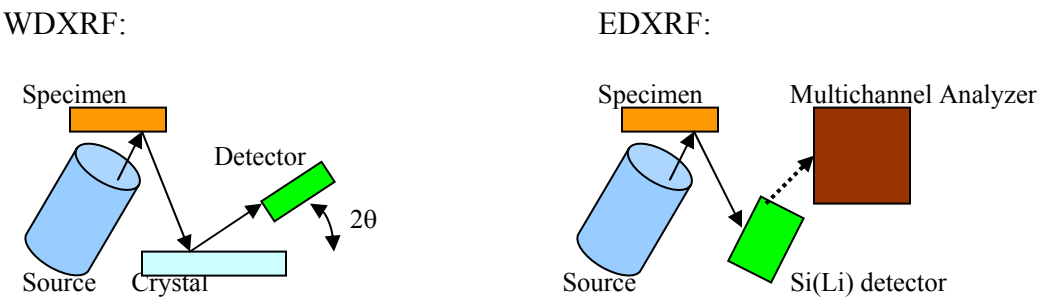


Figure 1-3. Comparison of WDXRF and EDXRF systems

EDXRF system uses a Si(Li) detector, which is made up of *p*-type silicon and lithium, creating a Schottky barrier contact. This produces a *p-i-n* junction diode. To limit the electrical noise, the diode is cooled by liquid nitrogen in most systems. Application of

a reverse bias causes charge removal from the silicon part. When hit by X-ray photons, the interaction results in electron-hole pair production. The charge created here will be transferred to a charge sensitive preamplifier. A charge loop incorporates the capacitor charge to produce an output pulse. For a Si(Li) detector, the electrical noise of 100 eV is present. For a Cu $K\alpha$ line, resolution of the Si(Li) detector (in EDXRF) is estimated to about 160 eV, while the same for LiF(200) and LiF(220) crystals (in WDXRF) can range from 10 to 32 eV.[1] As the analyte photon becomes more energetic, the difference in resolution between Si(Li) and LiF crystals decreases.

**Low Concentration Limit**

The lowest detection limit is usually defined as the concentration that is equal to a certain number of standard deviations of the background. There are a few things on which the lowest detection limit depends on. They are 1) the background counting rate (blank), 2) measurement duration, and 3) the spectrometer sensitivity (counts per unit concentration of the target element).

WDXRF has sensitivity of a few orders of magnitude greater than that of EDXRF. This difference comes from the difference in the counting rate. WDXRF, in general, can maintain counting rate of up to 1,000,000 counts per second, while that of EDXRF can go up to about 40,000 counts per second.[1] This difference rises from the fact that EDXRF detector receives signals all at the same time, while the detector for the WDXRF can see the signals only at preset locations.

**Qualitative Analysis**

EDXRF is particularly suited for analyzing unknowns or qualitative analyses. [1, 2, 6] If WDXRF is to do a qualitative analysis, it takes much longer due to the detector mechanism employed in WDXRF systems. To perform a qualitative analysis on a

WDXRF, the detector should be set so that it scans across certain range of angle (see Figure 1-2) to account for as much signal from the specimen as possible to ensure completeness of the data. The detector moves across the whole scanning range at a constant speed, which presents a problem, especially in detecting elements with low atomic numbers (low-atomic number elements require much longer time for accurate detection). In addition, WDXRF requires sequential scanning and a series of scanning with different conditions (to cover all range of elements) at one location, which automatically makes the time necessary per measurement longer.

## Quantitative Analysis Procedure

In previous sections, qualitative analysis by XRF was discussed. XRF is also suited for quantitative analyses, owing to its high sensitivity and flexibility to cover a wide arrange of samples. However, it is not free of errors, just like any other quantitative methods. The sources of error, both random and systematic, can be numerous, and it is important to minimize and control the errors. On average, an EDXRF would have a precision of approximately 0.25% to 0.5% for measuring a single, well-separated line.[1] In the following, the procedure for quantitative analysis is outlined.

### Random and Systematic Errors

In X-ray instruments, a major source of random error is the X-ray source (the high voltage source and the X-ray tube). Also, the actual counting step is subject to statistical errors. EDXRF systems are prone to full- or partial-line overlaps as well (if the elements of interest have lines that are closer to each other than the resolution of the equipment), which introduce another major source of random error. In some cases, the error in measurement can reach several percent. Modern systems include a software package in an attempt to assist users in dealing with this kind of error.

Standard deviations can be estimated by the following equation:

$$s = K \times \sqrt{(C + 0.1)} \tag{1-6}$$

in which $C$ is the analyte concentration, and $K$ is a constant that varies from 0.005 (for a very high quality measurement) to 0.05 (for a poor quality measurement). The value of $K$ is obtained directly from each system, and a reasonable value would be 0.02 to 0.03. The following table[1, 2] summarizes the sources of random and systematic errors.

Table 1-4. Sources of random and systematic error

| Source | Random | Systematic |
|---|---|---|
| Sampling | At discretion of sampler | - |
| Sample Preparation | 0 to 1% | 0 to 5% |
| Sample Heterogeneity | - | 0 to 50% |
| Excitation Source | 0.05 to 0.2% | 0.05 to 0.5% |
| Spectrometer | 0.05 to 0.1% | 0.05 to 0.1% |
| Counting Statistics | Time Dependent | - |
| Deadtime Losses | - | 0 to 25% |
| Primary Absorption | - | 0 to 50% |
| Secondary Absorption | - | 0 to 25% |
| Enhancement | - | 0 to 15% |

It should be noted that some systematic errors could be so large that careful monitoring of each step and careful calibration/correction are necessary to minimize these errors.

**Background Count**

For a quantitative analysis, the background count should always be taken into account, and the treatment of the background can influence the net count as well. A careful measurement of the background is just as important as the raw data when calculating the net count. A major portion of the background count comes from scattered source radiation. Since low atomic number elements have higher scattering than high atomic number elements, the background is much larger for low atomic number elements (or specimens with a lower average atomic number). As a rule of thumb, the background

varies as $1/Z^2$.[1] Depending on the shapes of the resulting spectra, different correction schemes are utilized. For example, there could be no significant background, background can be present but constant for a given peak, or the peak in question may lie in the middle of the rapidly changing background levels. To complicate things even further, two peaks that are close to each other can be overlapping. The following figures illustrate different scenarios of background calculations.[1.3]

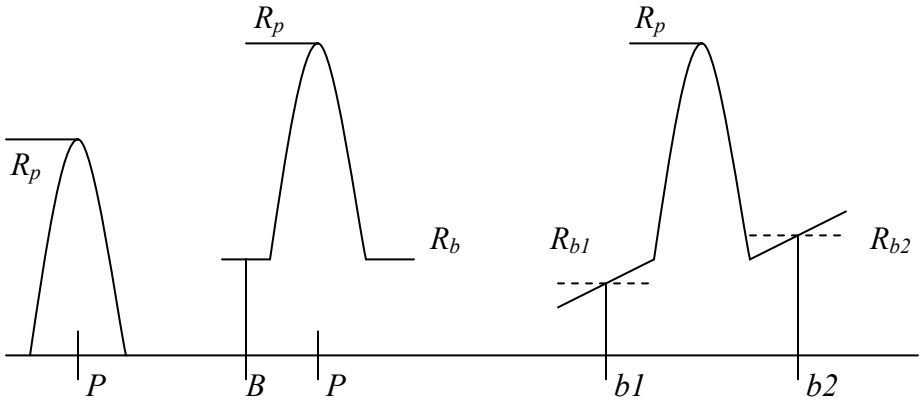


Figure 1-4. Peaks with: no background, with a constant background, and with varying background (from left to right)

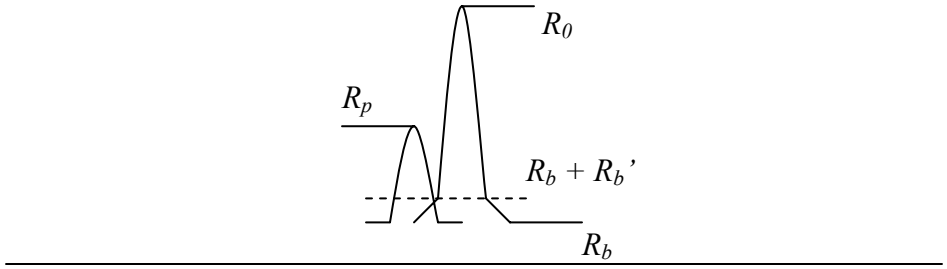


Figure 1-5. Peak overlapping with an adjacent peak

For a peak with no significant background, the net peak intensity $R_n$ is

$$R_n = R_p \tag{1-7}$$

For a peak with a constant background, $R_n$ is

$$R_n = R_p - R_b \tag{1-8}$$

For a peak with varying background, $R_n$ is

$$R_n = R_p - \left( \frac{R_{b1} + R_{b2}}{2} \right) \tag{1-9}$$

For a peak overlapping with an adjacent peak, an assumption has to be made. It is assumed that the ratio of the peak intensity of the interfering line to the intensity (at the interfering shoulder of the line) is constant. For this case, the net intensity becomes

$$R_n = R_p - K\left(R_0 - R_b\right) \tag{1-10}$$

The value of $K$ depends on factors such as degree of overlap.

The above scheme is the general approach. For EDXRF, a slightly different method is used.

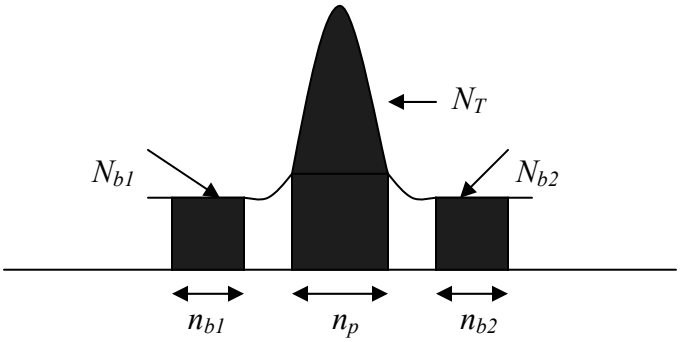


Figure 1-6. Peak illustration for EDXRF calculation of net peak intensity

In EDXRF, the correction is handled differently; instead of choosing a single peak location and its corresponding intensity, a band of peak is chosen. Likewise, a band of background on both sides of a peak of interest is chosen (shaded areas in Figure 1-5). In Figure 1-5, $N_T$ represents the peak counts (shaded area under the peak), $N_{b1}$ and $N_{b2}$ are the background counts on two sides, *nb1* and *nb2* are the ranges of background counts, and *np* is the peak range. The net peak counts are given by

$$N_n = N_T - \left( \frac{n_p}{\left(n_{b1} + n_{b2}\right)} \times \left(N_{b1} + N_{b2}\right) \right) \tag{1-11}$$

**Statistics (Counting Errors)**

X-ray generation is a random process with a Gaussian distribution.[3] For a Gaussian curve, a measured value of N would have a random error, $s_N$, which is equal to $\sqrt{N}$. Table 1-5 summarizes the meanings of these parameters for a Gaussian distribution.[3]

Table 1-5. Summary of Gaussian distribution

| Value Range | Probability of a Given Measurement to be in the Value Range |
|---|---|
| $N \pm \sqrt{N}$ | 68.3% |
| $N \pm 2\sqrt{N}$ | 95.4% |
| $N \pm 3\sqrt{N}$ | 99.7% |

From EDXRF net counting error $s_{net}$ can be estimated as

$$s_{net} = \sqrt{P} + B\left(1 + \frac{n_p}{n_{b1} + n_{b2}}\right) \tag{1-12}$$

where P is the net peak counts (same as $N_n$), and $B$ is the background counts.

**Matrix Effects**

During the data acquisition, elements can interact with each other, which makes some corrections necessary. Table 1-6 summarizes the possible matrix effects.[6]

Table 1-6. Summary of matrix effects

| Categories | Subcategories | Effects |
|---|---|---|
| Absorption | Primary | Atoms in specimen absorbing photons from primary source |
| | Secondary | Atoms in specimen absorbing characteristic analyte radiation |
| Enhancement | Direct | Atoms in specimen excited directly by primary continuum or characteristic radiation from source |
| | Analyte + one enhancing element | Analyte element in specimen excited by characteristic radiation from non-analyte element in specimen |
| | Third Element | A second non-analyte directly excited by source, which can excite the analyte element or the first non-analyte element, increasing enhancement by the first non-analyte element on the analyte element |

**Quantitative Low Concentration Analysis**

The definition of the lower limit of detection (LLD) is the concentration equivalent to two standard deviations of background counting rate.[2] The LLD for EDXRF is estimated to be

$$LLD = \frac{3}{m} \times \sqrt{\frac{R_b}{t_b}} \tag{1-13}$$

where $t_b$ is the total live time (net amount of time that the spectrometer is counting or collecting data), m is the sensitivity (in concentration), and $R_b$ is the background intensity.[1, 6] Note that both $R_b$ and m vary with the average atomic number of specimen. In general, the LLD of most XRF systems lies in the order of low parts-per-million level for most of the elements, while low atomic number (large wavelength region) elements have much higher LLD, suffering from low fluorescence yield and increased absorption effect.

**Quantitative Procedures**

The intensity of a characteristic radiation of a target element is related to its concentration, and there are many methods available to express the correlation. This relationship may not be linear, especially over a wide range of concentration. The major factors causing the non-linearity are matrix effects and specimen heterogeneity effects. If the specimen is homogeneous, then the major contributing factor to be considered is the interactions between elements in the matrix of that particular specimen. There are many methods developed to suppress errors arising from the many aspects of making measurements. The subsequent discussion focuses on single element methods.

The most traditional of all, type standardization is based upon the assumption that the slope of the calibration curve (concentration versus intensity) will remain constant,

provided that the concentration range is limited. The correlation between the parameters would look like

$$\frac{W_l}{W_h} = \frac{I_l}{I_h} \times \frac{\alpha_l}{\alpha_h} \times \frac{K_l}{K_h} \tag{1-14}$$

where subscripts *l* and *h* stand for low and high concentrations, *W* is the weight fraction of the target element, *I* is the line intensity, α represents the absorption effect, and *K* is the slope of the calibration curve.[6]

A method considered the most useful for a single element analysis in a known or an unknown matrix is the internal standard method. This method utilizes the addition of an element standard with a known concentration that has a wavelength similar to that of the target element. Replacing the subscripts with x for the target element and s for the standard, the above equation becomes

$$\frac{W_x}{W_s} = \frac{K_x}{K_s} \times \frac{I_x}{I_s} \tag{1-15}$$

This method is based on the assumption that $\alpha_x = \alpha_s$. The internal standard method is best used when the concentration of target element in specimens is less than about 10%.[6] This constraint comes from the fact that the internal standard added should have about the same concentration level as that of the target element. When the amount of the internal standard significantly exceeds the analyte concentration, the change in matrix will be considered significant enough to introduce errors.

Another method that is widely used, especially when the concentration of the target element is less than 5%, is the standard addition method.[6] This method can be considered an internal standard method where the standard element being added is the

same as the target element (also termed as *spiking*). For this method, the mathematical correlation between the intensity and the concentration becomes

$$\frac{W_x}{W_x + W_a} = \frac{I_x}{I_{x+a}} \tag{1-16}$$

in which the subscript *a* refers to the added standard. Thus, $I_{x+a}$ is the intensity of the specimen after the standard addition. This method also assumes a linear relationship between the intensity and the concentration. To be sure that this assumption is correct, standard addition step may be repeated twice.

CHAPTER 2
SAMPLE PREPARATION

There are numerous methods of sample preparation available to date.[3-5] The choice of sample preparation depends on factors such as sample matrix (gas, liquid, or solid), atomic numbers of target elements, target element concentration, and so on. This chapter discusses the sources of error, some examples of sample preparation procedures, with a focus on liquid sample preparations, and a review of preparation methods in use for XRF analyses.

## Sources of Error

### Statistics of Sampling

For accurate analyses, it is crucial to be sure that samples being measured are representative of the whole. To ensure this point, random sampling, or choosing samples without structured bias, is necessary.[6] However, it may be the case that the process of sampling itself is done in a highly systematic manner. Thus, a strict outline for quality control is required. Figure 2-1 defines the hierarchy of sampling.

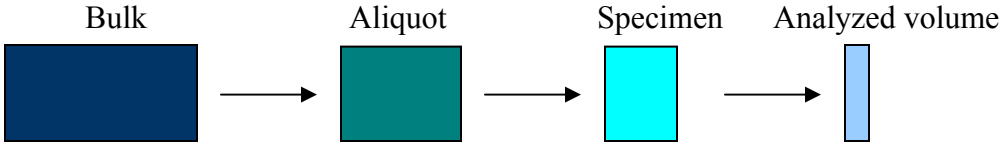


Figure 2-1. Hierarchy of sampling

Due to statistical nature of sampling and X-ray generation, knowledge of basic statistics will come in handy for XRF analyses.[6] Arithmetic mean, $\mu$, is defined as

$$\mu = \frac{1}{n}\sum_{i}^{n} x_i \tag{2-1}$$

where $\mu$ is the mean, $n$ is the number of independent measurements, $x_i$ is the $i$th measurement. Variance and standard deviation are used as a measure to describe the dispersion of the measurements about mean, $\mu$. The variance is given by

$$V = \frac{1}{n}\sum_{i}^{n} d_i^2 \tag{2-2}$$

where $V$ is the variance, and $d_i$ is the difference of $\mu$ and the $x_i$. The standard deviation, which is denoted by $\sigma$, is a square root of the variance. In a normal distribution of data, 95% of the data are contained in the $\mu \pm 2\sigma$ range.

**Sampling Errors**

There are two categories of sampling error: random and systematic. These terms were discussed previously for XRF systems error. The random error can be characterized by the variance only (the "spreading" of the data points), while the systematic error is characterized by the mean only. The systematic error can be highly precise but inaccurate, while the random error can be accurate but not precise. Sources of the systematic error include a false assumption about the samples by the analyst, which can contribute to a consistent but inaccurate result. Ideally, analysts would only see the random error. In practice, the systematic error is difficult to identify without some knowledge of the mean. This fact gives importance to the comparison of data. Data comparison can be considered as a means for quality control, and realized by employing different methods to achieve the same. Inter-laboratory comparison of results is another way to effectively control the quality of the analyses.

To control sampling errors, there are many materials properties to consider, such as the particle size for powder samples.[6] Particle size of powder samples can affect a wide

range of analytical results. During shipment, the container of some powder sample can vibrate, which can promote the segregation of particles with different sizes. So, if an analyst simply takes a scoop off the top of the container and assumes that it is representative of the bulk, a significant systematic error can be introduced. For liquid analysis, however, homogeneity is assumed in most cases, as long as the samples are free of solids and well mixing is ensured. [1,2,6]

Since the XRF is a nondestructive method of analysis, measurements can be repeated on a single sample. Doing so provides a way to test the system consistency. Sampling can also be duplicated. By definition, replication refers to the drawing of several samples from the bulk, and preparing them separately for analyses. This method is one way of verifying that the drawn samples are indeed representative of the bulk. One indication of biased sampling is the observation of *outliers* (also called runaways). Deciding whether a data point is an outlier or not can be problematic, especially when building a calibration curve. Usually, if a data point deviates from the mean value by more than $3\sigma$, it is safe to discard the data point as an outlier.[6]

## XRF Sample Preparation Procedure

XRF samples for an analysis are expected to be similar to one another (particle size, mass attenuation coefficient, density, homogeneity, *etc.*) for consistency and error minimization. Thus, sample preparation procedures are required to produce samples that are consistent in quality, in order to minimize the systematic error. It is better if the procedures are inexpensive and rapid. Ideally, analyzed specimens are representative of the bulk, and are stable before and during the sample preparation and analyses. Otherwise, pretreatment of samples may be necessary.

**Pretreatment of Samples**

Whether to pretreat specimens depends on the physical form of the received specimens. Direct analysis is by far the best option, since it requires no preparation time, and there is no concern of error introduction during the pretreatment step. There are issues to consider, which make the direct analysis difficult. These issues include heterogeneity of the as-received sample (non-uniform particle size, small sample size, sample composition heterogeneity, *etc.*). The following chart[6] can be used to determine what should be done to certain types of samples before analyzing them.

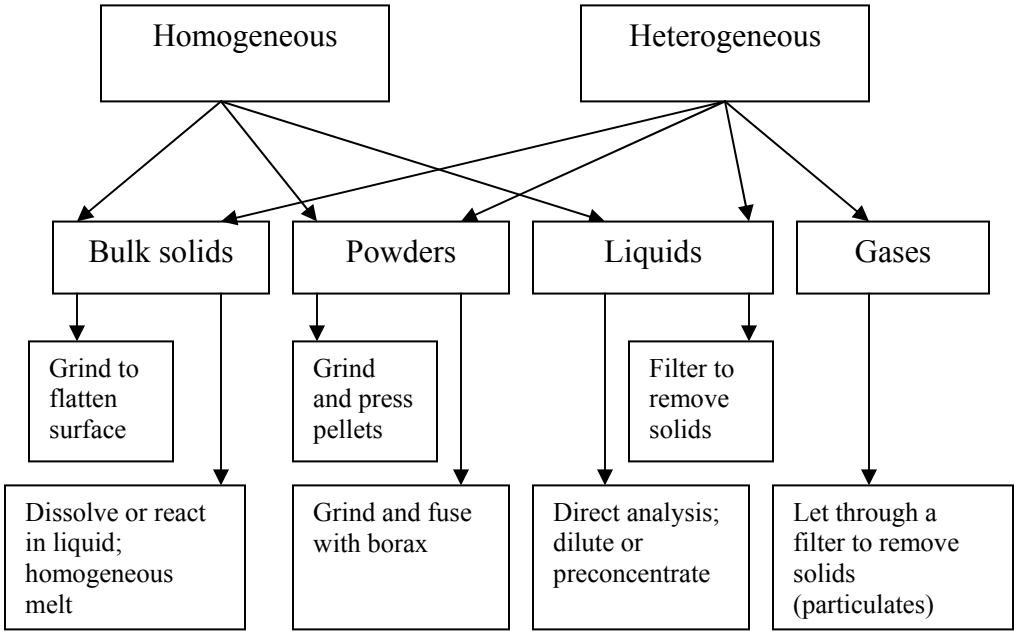


Figure 2-2. Pre-analysis treatment choices for different forms of samples

The pretreated samples can then be measured by XRF. During the analyses, there are a few more things to consider for error minimization.

**During the Analysis**

Vertical positioning of specimens inside an XRF is controlled by the system. Each system has its own sample mounting area, which is the best position with respect to the X-ray tubes and other parts that are vital to analyses. Horizontal positioning is controlled

by the analyst. This factor can influence the results dramatically in some cases. Depending on the location at which the incident beam falls, some compositional heterogeneity can contribute to variations in results.

Another concern during an analysis is the possibility of the specimen decomposition due to irradiation by an X-ray beam. Materials that are prone to this include some polymers. Also, damp specimens, when irradiated with a high energy X-ray beam, can cause ozone production (detected by the smell of the ozone gas).[6] Production of ozone gas in the sample chamber can promote the oxidation of organic specimens. To prevent unwanted chemical reactions during analysis and to reduce error size, pretreatment procedures should be considered to best suit the different sample types.

**Liquids and Solutions**

For dilute samples, preconcentration may be necessary to bring up the concentration of the analyte in question. This approach is necessary when: the concentration is close to or below the lowest detection level of the analytical instrument, or a measurement of dilute samples bears the possibility of having a significant error. When chosen to preconcentrate a sample, a large quantity of the original sample should be available. Preconcentration can offer a solution for liquid samples, whose analyses are otherwise difficult due to matrix effect and scattering.

Some examples of preconcentration method include the use of ion exchange resins. The use of ion exchange resin is one of the most studied methods of preconcentration. Ion exchange resins have functional groups fixed onto a solid substrate to extract the ions of interest. The success of this method depends on the ion recovery rate of the resin, or the affinity of the ion-exchange material to ions.

Ion exchange resins are chosen based on their compatibility with the ions of interest. The analyte solution is passed through a layer of ion exchange resin, eluted, and then evaporated onto filter paper discs. The discs are analyzed directly on the XRF. This method has one great advantage: the sample to be analyzed on XRF is so thin (tens of microns thick) that matrix effect is minimized. In some cases, use of filter paper discs loaded with the ion exchange resin was proven successfully (the procedures called for several passing of the analyte solution through the filter paper disc to ensure complete extraction). Bernardo *et al.*[8] investigated the use of cation exchange papers for successful extraction of cationic elements such as Al, Fe, Mn, Zn, and Cu. The analyte solution was passed through a single filter paper disc several times. Van Grieken *et al.*[9] used the Chelex-100 ion exchange membrane, under 2 to 3 bar of pressure, to extract trace metals in water. The filtration process took about 20 minutes for a 200-mL water sample. Minkkinen[10] used cellulose phosphate paper (ammonia form) for uranium determination, and achieved a detection limit of 0.3 μg in a 100-*s* counting time. The filter paper disc was analyzed directly. Alternatively, the ion exchange resin loaded with the element of interest can be directly measured by the XRF. In that case, the resin is measured as is or it can be pelletized.[6]

Though considered ideal, direct analysis is rarely possible with liquid samples. When the X-ray is irradiated onto liquid samples, absorption and scattering occur (especially in water sample matrix) that the background signal hinders the lines of interest. In this case, the evaporation method can be utilized to avoid the liquid matrix issues altogether. Evaporated specimens become easier to manage, and spillage onto the

analyzer can be prevented. By completely eliminating the liquid, the sample that is not otherwise analyzable on the XRF can become a candidate for XRF analyses.

When the amount of sample available for analysis is very small, care should be taken to ensure that the output signal is larger than the background. Typically, the irradiation area for an X-ray spectrometer is about 5 $cm^2$, and the penetration depth is approximately 20 μm. Therefore, no matter how much sample is put into a sample cup, the X-ray "sees" a very small portion (on the order of 50 mg) of the sample for each analysis.[6] The smallest amount of samples required for an analysis is about 0.005 mg, when the sample is uniformly spread over the X-ray irradiation area.

There are many potentially measurement-hindering aspects in sampling, sample preparation procedure, and XRF measurements. All aspects need to be considered closely to optimize the analysis conditions. The adaptations can lead to new applications of existing procedures as well.

## Recent Applications of XRF

XRF is a convenient, accurate, and versatile instrument for qualitative and quantitative analysis. XRF is used in a variety of areas, and there continue to be many innovations and new developments.[11-13] Environmental, archaeological, and forensic studies are the areas in which XRF is frequently used. In the following, examples of these new developments are discussed.

### Laboratory Procedure

Analytical methods require contaminant-free environment, especially when working with dilute samples. Each step should be monitored with great care to minimize impurity introduction.

Every step that calls for water usage (such as dilution or washing) has a potential of contamination. Therefore, ultrapure (or nanopure) water should always be used for trace metal detection procedures. Hoelzl *et al.*[14] suggested the ultrapure water quality be monitored weekly in a high-throughput laboratory on a weekly basis. Inductively coupled plasma mass spectrometry (ICP-MS) was used to monitor the impurity concentrations in ultrapure water down to the 10 parts per trillion (ppt, or ng/L) level. Dabouret and Kano[15] point out that Si and B are the first two elements in most cases to contaminate water. They described how the latest water purification system with reverse osmosis/eletrodeionization technologies could alleviate this issue. Sutarno and Steger[16] outlined the experimental procedure to verify the accuracy and precision of analytical data and methods by using the certified reference materials (CRM).

The effect of sample bottle materials and acid washing of bottles on specimens was studied by Reimann *et al*.[17] This group looked at five different bottle types: high density polyethene (HDPE), polypropene (PP) by two manufacturers, fluorinated ethane propene copolymer (FEP), and perfluoroalkoxy polymer (PFA). Each bottle type was used to store groundwater samples. The ground water samples were then analyzed by ICP-MS for a variety of elements present down to the ppt levels. Also, for HDPE and PP bottles, parallel samples were stored in unwashed, factory-new bottles and acid-washed, factory-new bottles. The group concluded that acid washing has no apparent benefit. For PP bottles, acid washing even introduced the impurities Pb and Sn to a significant level. The bottle material had no influence on the results for many elements. As an exception, Cr levels from samples stored in HDPE bottles were significantly higher than it was before storage. This was observed for both unwashed and acid-washed bottles alike. Based on

the observations, FEP or PFA were concluded to be only slightly better choice for sample storage than PP and HDPE. Thus, cheap, factory-new HDPE bottles were concluded to be the best choice for storing ground water samples for ICP-MS analysis.

The effect of filtration was studied by the same group.[18] Filtration is an extremely slow process (especially at the <0.10 μm level). If such a time-consuming step were to be justified, there should be a significant difference between filtered and unfiltered specimens. The filtration step is also believed to introduce contamination from the filter paper, causing removal of some elements by colloid retention, and solid precipitation on the filter. The same groundwater samples used for the bottle material analysis were used to compare the filtered (<0.10 μm and <0.45 μm) and unfiltered specimens. The filtered and unfiltered samples were then analyzed by the ICP-MS. The result suggested that filtration does not affect the concentration of most of the 62 target elements. One exception is Sn in that filtration would actually introduce contamination. For samples without particulates, filtration does not have a profound effect, thus additional effort of filtering samples may not be justified in some cases.

To verify the results obtained by XRF, especially when dealing with low concentration samples as discussed above, it is always recommended that other means of analysis be employed on the same set of samples. Nguyen *et al.*[19] investigated a procedure to determine Hg levels in environmental samples. First, the effectiveness of the procedure was verified by comparing the XRF results on a set of standard samples with that from cold vapor atomic adsorption spectrometry (CV-AAS). The results from EDXRF and CV-AAS were concluded to be in good agreement. The results were in good

agreement with the certified values as well. The procedure was applied to detect Hg levels in coal, vegetation, fish, sediment, and human hair.

Up to this point, examples of a variety of different samples being measured by XRF were already mentioned. Even more applications of XRF on gas, solid, and liquid samples are reviewed in the following.

**Gas and Solid Analysis**

There are many established methods to analyze gas samples by EDXRF. Kurunczi *et al.*[20] tested the effectiveness of Ag-coated quartz fiber filters developed to collect Hg from flue gas in a laboratory setting. On an average, 88% mercury collection efficiency was reported. Kallithrakas-Kontos *et al.*[21] analyzed the air quality near the area of Ptolemais (Greece), where lignite power plants are in operation. Aerosol filters were collected ten years apart, and analyzed by radioisotope excited XRF for 17 elements, including Pb. The result was verified by AAS. The composition of vehicle exhaust particular matter (PM) was analyzed by EDXRF.[22] Exhaust was run through filters, and the filters were analyzed for 38 elements. The results averaged between 3 to 9% of PM10 mass from gasoline and diesel engines.

XRF can also be used for analyzing numerous solid specimens. Aisueva and Gunicheva[23] developed a nondestructive method for soil/sediment analysis for major and trace elements. Specimens were simply dried at 105 °C, followed by XRF analysis. The results were corrected for matrix effect due to the heterogeneity of specimens. Mendoza *et al.*[24] used EDXRF to analyze pollutants in microalgae, marine algae, marine sediments and corals from the Havana (Cuba) area. The specimens were prepared by using a plastic resin. Focus was given to heavy metal presence, as the represented specimens are

considered pollution indicators. Katahira *et al.*[25] made observations on surface soil and plant samples collected in various parts of Kyoto (Japan). Metal concentrations in the specimens were determined by XRF. The study confirmed that the XRF method is well suited for quick monitoring for this purpose, owing to simplicity in sample pretreatment. Szaloki *et al.*[26] looked at the elemental composition of lake bottom sediment. Core samples were taken, divided into 1cm thickness, dried, homogenized, and digested with nitric acid and hydrogen peroxide for inductively coupled plasma atomic emission spectrometry (ICP-AES) analysis for Ca, Fe, Mn, Sr, and Ba content. The undissolved portions of the samples were analyzed by EDXRF (Si, Ca, K, Ti, Zr, and Y). Ro *et al.*[27] investigated the heterogeneity problems associated with EDXRF analysis. A reference material (IAEA-413, which is a single cell algae grown with toxic elements) was used for consistency.

**Liquid Analysis**

In most cases, liquid samples require some form of preconcentration step for XRF analysis. There are several ways to realize this, and commonly used procedure include extraction of elements in interest through the use of chelating agents, analyzing filter paper discs that are loaded with liquid samples, or combinations of both. De Vito *et al.*[28] developed a stable chelating resin, which is prepared by adsorbing (o-[3,6-disulfo-2-hidroxy-1-naphthyazo]-benzenearsonic acid), or thorin, on a macroporous resin Amberlite XAD-7. This resin is effective in preconcentration of trace rare earth elements such as Sm(III), Eu(III), and Gd(III). The preconcentration factor achieved was 500, and the loaded resin was analyzed by XRF. Latva *et al.*[29] used activated charcoal to adsorb As (III) and As(IV) in aqueous solution. The activated charcoal loaded with As was measured directly by EDXRF. Trace amounts of Ga and In in geological samples were

successfully preconcentrated with macroporous resins Amberlite XAD-4 and XAD-7, loaded with 5-phenylazo-8-quinolinol (5-PHAQ).[30] Concentrations were determined by using the calibration curves. The detection limits obtained were 98 ppb for Ga and 81 ppb for In. Trace Se and As preconcentration was achieved by solvent extraction.[31] This method was developed to determine Se and As levels in drinking water. The preconcentrated specimen was measured by XRF. McComb and Gesser[32] utilized amidoxine chelating groups covalently bound to the surface of a piece of cloth for determination of various trace elements (Pb, Cu, Zn, Cd, Mn, Fe, Mg) in water. The prepared specimen was analyzed by WDXRF, and then acid-extracted samples were measured by inductively coupled optical emission spectrometry (ICP-OES) for comparison. WDXRF and ICP-OES results were in good agreement for Pb measurement.

**Uranium Detection Method**

As mentioned above, XRF is used to measure the amounts of many elements in a wide variety of sample matrices. Uranium, too, can be measured by XRF. U is the heaviest element that can be measured on XRF. There are numerous studies done to detect U in different matrices by XRF, but here the focus is given to U detection in water.

Dewberry[33] outlined a method for determination of total U amount in solutions. The concentrations of U examined in that study are 1 to 15 g/L (U solutions in 2 M nitric acid). 5 mL aliquots of liquid samples were pipetted into plastic vials, then each was spiked with 50 μL of 40μCi/mL $^{109}$Cd source. The U L-line measurements were used to determine the amount of U.

Carvalho *et al.*[34] developed a method to determine U concentration in water at ppb levels by WDXRF. Earlier, Carvalho *et al.*[35] developed the powdered polyurethane foam

(PUF) preconcentration method for Ga determination. The Ga method was applied for U determination with some changes. This method is the solid phase extraction (SPE) of U(VI) as the salicylate complex using PUF. The procedure is outlined below.

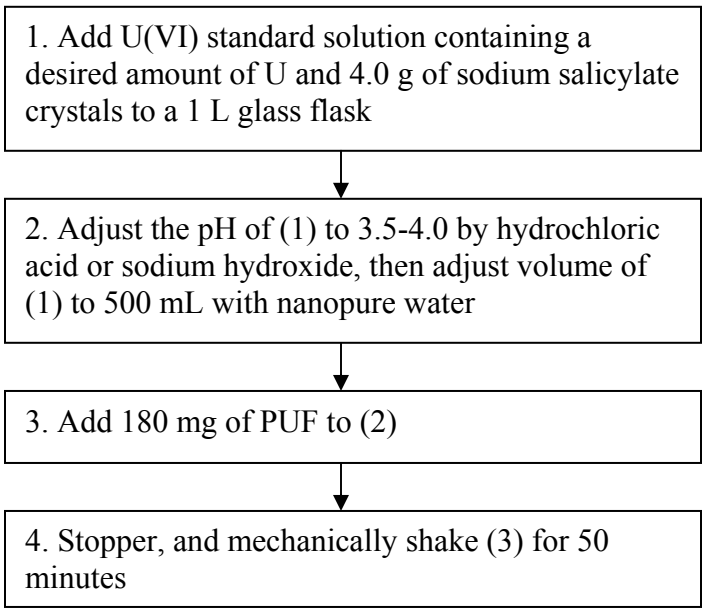


Figure 2-3. U adsorption procedure by PUF method

All parameters involved in this procedure were optimized by carefully examining the effect of each parameter to the WDXRF intensities of the resulting specimens. Glassware was washed with nitric acid beforehand. PUF was first soaked in 6 M hydrochloric acid, and then dried. The PUF specimen was prepared as follows.

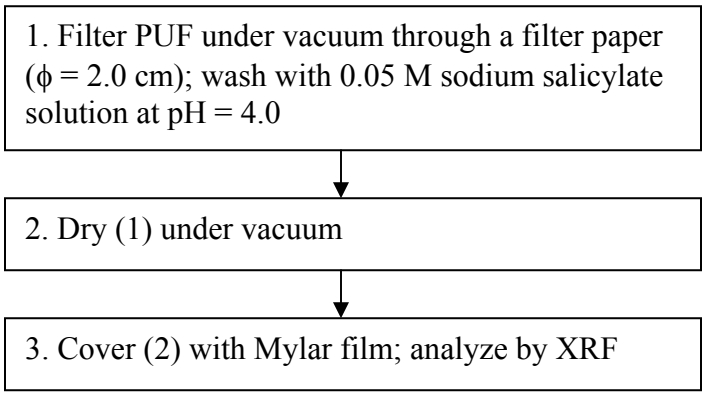


Figure 2-4 Specimen preparation

The detection limit was reported to be 5.5 ppb for this method. The effect of the presence of foreign ions was also discussed. In addition, comparison between amounts of U found by PUF and the certified values were reported. Results were reported in percent recovered, with the certified values of U concentration (from 0 to 175.2 ppb U in sea water) as 100 percent. All PUF results were within 6% of the certified values.

Therefore, the PUF method can be considered accurate and useful for U detection. However, there are several issues to be pointed out. First of all, the linear dynamic range reported is from 10 to 280 ppb. Although this method is suited for dilute samples, the range over which the method is useful is rather narrow. Secondly, although the XRF analysis itself takes only a few minutes for this method, it takes almost two hours to prepare samples (to cover all steps outlined in Figures 2-3 and 2-4). This method is not suited for analyzing a large number of samples. Lastly, the procedure has many steps, and use 500 mL of liquid to prepare a single sample. A large quantity of waste water (possibly radioactive, since a small amount of U(VI) may still remain) is generated. Therefore, this method is for small batch of liquid samples, whose U concentration is well below 0.5 parts per million (ppm). For large batch of liquid samples with U concentration above 1 ppm, an alternative method was desired.

Turner *et al.*[36] addressed a sample preparation method called microsample X-ray analysis (MXA). A 50-μL droplet of sample was deposited on an ultrathin (0.15μm) X-ray window film support to dry completely. The resulting residue was then analyzed by XRF. Samples (river water taken from Provo River spiked with a known amount of trace elements to certified reference materials) with various elements with a wide range of concentrations were examined. The MXA results were then compared to those by ICP,

graphite furnace atomic absorption (GFAA), and CVAA. Some samples were also sent to a commercial lab for comparison. To verify the effectiveness of MXA, NIST (Gaithersburg, MD) Standard Reference Material SRM 1643d Trace Elements in Water was analyzed. MXA results were expressed in % recovered, with respect to the certified concentration. SRM 1643d has almost 20 elements at concentrations ranging from 21 ppb (Cu) to 31 ppm (Ca). The MXA results were all within 17% of the certified values (except for Sb with 131% recovery, and V with 66% recovery). MXA results from river water samples were all within 12 to 14% of the known concentrations. Overall, MXA results were in good agreement with ICP, GFAA, and CVAA.

It was concluded that this method is suited for determination of metal ions at low concentrations in environmental waters. The error size of approximately 15% can generally be tolerated. The procedure is extremely simple, inexpensive, and rapid. MXA is ideal for treating a large number of samples with a wider range of concentrations (from ppb to ppm for some metals), accurate to within about 15%.

Turner *et al.*[36] did not include U in its analysis. Thus, the MXA procedure was adopted for determination of U(VI) in water. Subsequent chapters in this work illustrate the details of how the MXA sample preparation procedure was adapted for U analysis of water specimens.

# CHAPTER 3
# EXPERIMENTAL PROCEDURE

## MXA Sample Preparation Procedure

### Standards, Reagents, and Supplies

A 1000-ppm U(VI) in 2% nitric acid solution was obtained from High Purity Standards. It was diluted to different proportions by 5% nitric acid-nanopure water to make standard solutions. Acidification was necessary to control the residue diameter.[36] Seven concentrations ranging from 0 to 20 ppm U(VI) were chosen to construct the calibration curve.

Table 3-1. Concentrations of U(VI) used for calibration curve

| [U(VI)] (ppm) | 0 (blank) | 2 | 4 | 8 | 10 | 15 | 20 |
|---|---|---|---|---|---|---|---|

Nanopure water used for dilution throughout this study was obtained from Engineering Research Center at the University of Florida (generated by a Barnstead water purification system; filter pore size = 0.02 μm) in Gainesville, FL. Concentrated nitric acid, trace metal grade, used for acidification, was obtained from Fisher Scientific. For this study, glass vials were used for short-term storage of the analyte solutions, and HDPE bottles were used for sample preparation and dilution.

XRF sample cups for the analysis were purchased from Chemplex Industries (Stuart, FL). Model 1330 (outer diameter = 32 mm, height = 23 mm, aperture = 25 mm, and reservoir capacity = 3 cc), double open-ended cups with resealing venting and overflow reservoir snap-on closure, was chosen for this study. The outer diameter size of this model was appropriate for the method, because it is approximately 0.7 mm smaller

than the diameter of the sample holder on the autosampler of the EDXRF. This extra space allows for horizontal adjustment of the sample position, ensuring that the analyte residue is aligned with the X-ray beam location. The snap-on caps for the sample cups were not used during the measurement, since the measurement was performed in air, and the position of the residue had to be visible to the operator.

The 3.6 μm–thick polyester film was used as the X-ray window, which was supplied with the spectrometer. Since the target element is U for this study, whose L$\alpha$ X-ray energy is approximately 13.61 keV, any polymer film under 10 μm of thickness can allow complete signal transmission. The film was loaded onto sample cups, and held tight with an outer ring of the sample cup.

Eppendorf and Finnpipette micropipetters (Fisher Scientific) of various volumes were used for dilution and dispensing of the samples throughout the study. Table 3-2 shows the micropipetters used in this study, accompanied by their approximate accuracy in ±% (reported in the Fisher Scientific catalog).

Table 3-2. Micropipetters used

| Brand and volume | Eppendorf 500 μL | Eppendorf 50 μL | Finnpipette 5 – 50 μL | Finnpipette 100 – 1000 μL | Finnpipette 2 – 10 mL |
|---|---|---|---|---|---|
| Inaccuracy (±%) | 0.6 | 0.7 | 3 – 0.6 | 1.5 – 0.5 | 0.4 - 0.3 |

All (glass) volumetric flasks used were of class-A, whose tolerance levels are ±0.2, 0.1, and 0.08% for 10-mL, 50-mL, and 100-mL flasks, respectively.

**Instrument**

The dried sample residues were analyzed on Philips Analytical (Natick, MA) PW4025 MiniPal EDXRF Spectrometer. The instrument is controlled by a personal

computer (software was supplied with the EDXRF). Table 3-3 summarizes the major specifications for the instrument.[37]

Table 3-3. Specifications of MiniPal EDXRF

| | |
|---|---|
| Detectable elements | Na to U |
| Dimensions | Height: 21.5cm, Width: 53.0 cm, Depth: 49.5 cm |
| X-ray beam stop | Reference position (alloy of Al and Cu);<br>Cu for gain correction<br>Al/Cu for instrument energy calibration |
| Measuring medium | Air or He (for improved sensitivity for Na to K detection) |
| Detector | Si-PIN detector; thin Be window |
| Detector cooling system | Peltier (thermoelectric) system; no liquid N necessary |
| X-ray tube | Power: 9 W<br>Voltage: 4 to 30 kV<br>Current: 1 to 1000 μA<br>Anode material: Rh |

The instrument is encased in Al seal for safety. X-ray generator has a safety switch, which turns itself off automatically when the lid is opened.

Figure 3-1. Philips Analytical MiniPal EDXRF

The instrument-specimen configuration is illustrated in Figure 3-2 below. The incident X-ray is generated by the X-ray tube (anode material: Rh), and then the beam is filtered. There are several filters available to choose from. The Ag filter was chosen for this study to allow the widest range of characteristic beam energies to be considered. The incident beam hits the underside of the specimen. Upon generation of characteristic rays, the Si-PIN detector receives signals to be displayed as output. The following EDXRF settings were used for all measurements: voltage at 30 kV, the current at 300 μA, the measurement time at 300 s, usage of Ag filter, and U and Th were chosen as target elements. Th was chosen to track possible contamination and/or need for data corrections (as discussed in Chapter 1). The location of L series peaks for Th are close to those of U, thus Th was the ideal choice for this purpose.

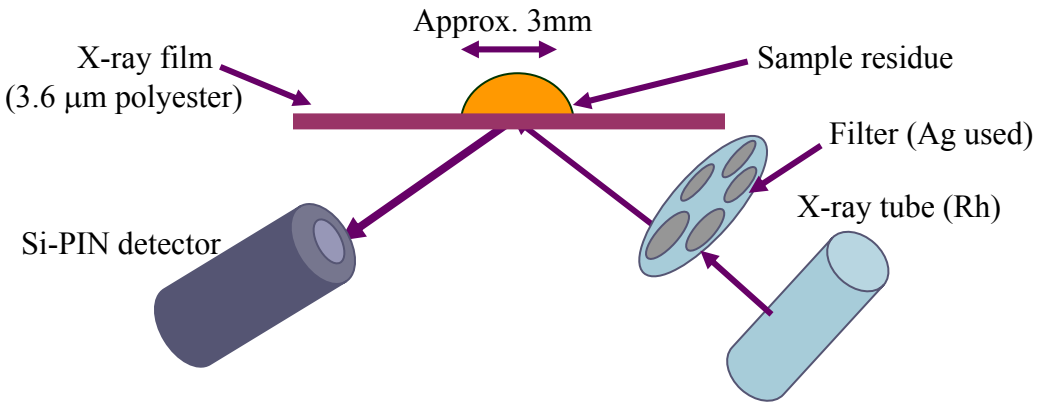


Figure 3-2. Instrument-specimen configuration for MXA analysis

**MXA Sample Preparation**

MXA samples for EDXRF analysis were prepared based on the procedure outlined by Turner *et al.*[36] XRF sample cups were preloaded with polyester X-ray window films in a fume hood to minimize dust collection. Presence of dust dramatically affects the residue diameter (most often a dust particle becomes a foreign inclusion in the residue, which increases the residue size to an unfavorable level, and also contaminates the residue

itself). The diameter of the dry residue should be kept under a few millimeters, or smaller than the X-ray beam spot size.[36] Three samples were made for each concentration (one 50-μL deposit per sample cup), and each sample cup was measured on the EDXRF three times. The volume of the specimen solution used to make one sample was made consistent by the use of a fixed-volume, Eppendorf 50-μL micropipetter. The averaged data of the total of nine measurements were used for the calibration plot. The following figure describes the procedure in steps.

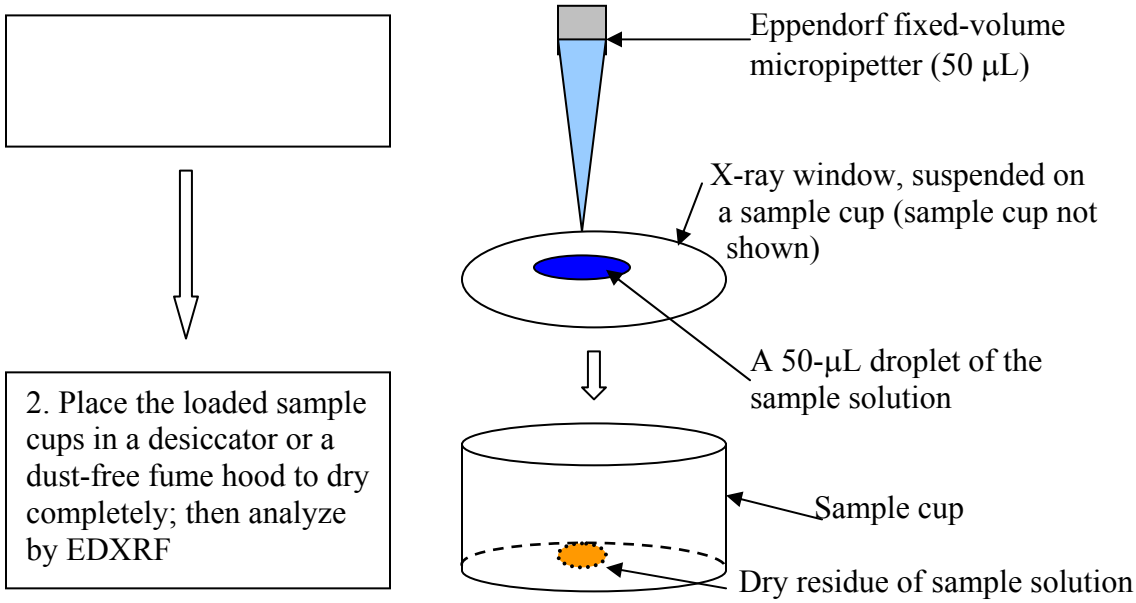


Figure 3-3. Sample preparation procedure

Samples with the following U concentrations were measured: 0 (blank), 0.5, 1, 5, 10, 15, 25, 50, 100, 200, and 500 ppm. The samples were obtained by diluting the 1000-ppm U(VI) standard solution in appropriate proportions.

To verify the effectiveness of the MXA sample preparation method, UA-3 uranium analyzer was used to measure the same set of U sample solutions. A brief discussion on UA-3 is given below.

## Comparison – Uranium Analyzer

### Background

UA-3 Uranium Analyzer, manufactured by Scintrex (Denton, TX), was used to verify the MXA data. Uranium analyzer is an electro-optical instrument for trace U measurement in liquids. A uranium analyzer utilizes the fact that uranyl salts, under ultraviolet (UV) excitation (from a small nitrogen laser with wavelength at 337 nm), emit a green luminescence. This luminescence can be measured quantitatively to determine the concentration of uranyl ions. The emission spectrum is distinct and characteristic, which consists of three peaks (approximately at 494, 516, and 540 nm). Uranyl complex formation is achieved by the addition of a buffered inorganic complexing agent, FLURAN (a dilute sodium monophosphate-sodium pyrophosphate solution). FLURAN converts different forms of uranyl ions present in the sample to a single form with a high luminescent yield.[38] It should be noted that the presence of foreign ions (such as Fe and Mg) in excess can suppress the luminescence intensity. To compensate for the presence of potentially interfering species such as organic compounds, which is also known to suppress the uranyl luminescence, a filter is placed to block the luminescence from organic species. In addition, the difference in the lifetime of the luminescence of uranyl complex and that of organic species was considered. The interfering organic-matter luminescence is extremely short-lived (about 4 ns), as opposed to the uranyl luminescence decaying gradually. Thus, the photomultiplier was made to accept a delayed signal to indicate only the intensity from uranyl complex.

### Instrument

The UA-3 has the lowest detection limit of 0.05 ppb, and is able to measure up to 20 ppb. The estimated error is about ±15% at 1 ppb and above.[38] Each measurement

requires 5 to 6 mL of the sample, and this sample volume is expected to be consistent (the use of micropipetters is recommended). Quartz cells are used as sample containers. The machine and the background noises are compensated by adjusting ZERO and BALANCE controls, respectively. There is no pretreatment of samples required, provided that the U concentration is between 0.05 ppb and 20 ppb, the presence of interfering species are limited, and the acidity in the sample is less than 0.01%. Otherwise, dilution or preconcentration (and neutralization, if applicable) may be necessary.


Figure 3-4. Uranium analyzer Scintrex UA-3

**Measurement Procedure**

Reagents and supplies used here were of the same quality as those for MXA sample preparation-EDXRF analysis. For increased accuracy, the standard addition method was employed. This method takes two readings total: first, intensity from the sample alone, followed by taking another reading after the addition of a small amount (5 to 50 μL, volume measured by Finnpipette adjustable micropipetter) of fairly concentrated (500 ppb, 1, or 10 ppm) standard solutions. The amount of the standard addition was made

small to minimize the change in the original sample matrix. The volume of the standard addition depends on the estimated original amount of U present in the sample. Ideally, the amount of U added to the sample should be approximately equal to the amount of U originally present in the sample. This ensures an accurate measurement.

The power switch was turned on, and then left on for 4 minutes for the laser generator to warm up. When the "LASER READY" indicator came on, the LASER was turned on. The laser was allowed to stabilize (4 minutes). ZERO control was used to compensate for the machine noise (adjusting the deflection of the needle back to zero). A 4.6-mL aliquot of sample was then transferred to a quartz sample cell. A Finnpipette micropipetter (2-10 mL adjustable) was used to consistently measure the sample volume. The instrument was zeroed, with the sample cell in the chamber and the laser incident on the sample cells, by adjusting the BALANCE control. FLURAN was then added (0.8 mL for each sample; volume measured on a Finnpipette 100 – 1000 μL adjustable micropipetter) to the sample. The sample cell was sealed, and inverted a few times to ensure mixing. The sample-FLURAN mixture was then measured (this is the first measurement, $V_1$). After that, a small amount of concentrated standard solution was added (500 ppb and 1 ppm standards were used; the volume of standard addition was varied, depending on the first reading $V_1$, as discussed previously). Again, the sample cell was inverted a few times to ensure well mixing. The sample cell was put back into the chamber to take the second reading, $V_2$, with the standard addition. The U concentration, *Z*, can be calculated as below.[38]

$$Z = \left( \frac{V_1}{(V_2 - V_1)} \right) \times \left( \frac{v_{standard}}{v_{sample}} \right) \times [U_{standard}] \qquad (3\text{-}1)$$

where $v_{standard}$ is the volume of the standard addition in mL, $v_{sample}$ is the volume of the original sample used (always 4.6 mL for this study), and [$U_{standard}$] is the concentration of the standard added in ppb. For example, if $V_1$ is 0.28, and $V_2$ is 0.49 with 5 μL of 1 ppm U standard added, then the U concentration Z will be equal to

$$Z = \left(\frac{0.28}{0.49 - 0.28}\right) \times \left(\frac{5 \times 10^{-3}}{4.6}\right) \times 1000\, ppb = 1.45\, ppb \tag{3-2}$$

The same known samples measured by MXA-EDXRF method were diluted by a factor of 1,000 to 100,000 with nanopure water. They were analyzed by the standard addition method on the uranium analyzer for comparison to MXA results.

CHAPTER 4
RESULTS, DISCUSSION, AND CONCLUSION

## Results and Discussion

### MXA calibration

A calibration curve was constructed for the MXA method. Seven standard solutions (0, 2, 4, 8, 10, 15, and 20 ppm U(VI)) were analyzed by the MXA-EDXRF method. All of the XRF spectra obtained indicated that there is no significant amount of background. The raw intensity was equal to the net intensity. Figure 4-1 is a typical EDXRF scan of a sample prepared by MXA method (1000 ppm U), showing that there is practically no background present.

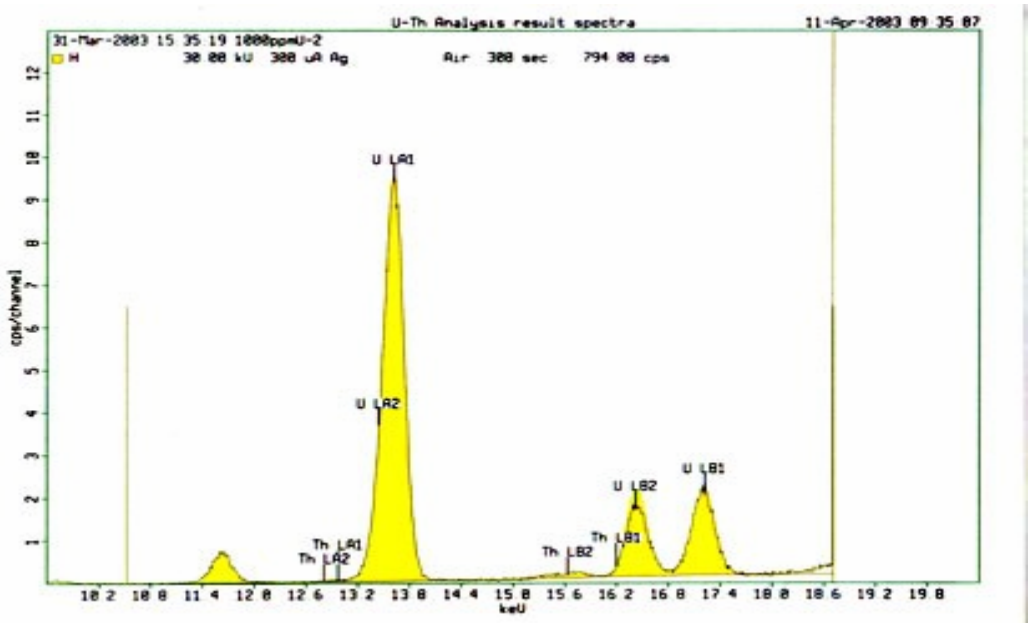


Figure 4-1. An XRF scan of MXA sample (1000 ppm U standard)

As Figure 4-2 shows, the calibration curve obtained was linear with the equation

$$y = 0.364x + 0.21 \qquad (4\text{-}1)$$

with $r^2 = 0.98$. As mentioned in the previous chapter, each point is the average of nine measurements (three samples were made out of each U(VI) concentration; each sample was measured three times under the same condition). The error bars represent the 95% confidence intervals for each data point. The size of error appears to have no correlation with the U concentration, for no distinct pattern was observed. The concentration range was limited to 0 to 20 ppm, since the linearity of the calibration curve cannot be certified over a larger range (as discussed previously). Studies on environmental waters (mostly dilute aqueous U samples with other trace metals present), for which this work was mainly intended, rarely calls for concentrations higher than 20 ppm. Thus, the concentration range for the calibration curve was appropriate.

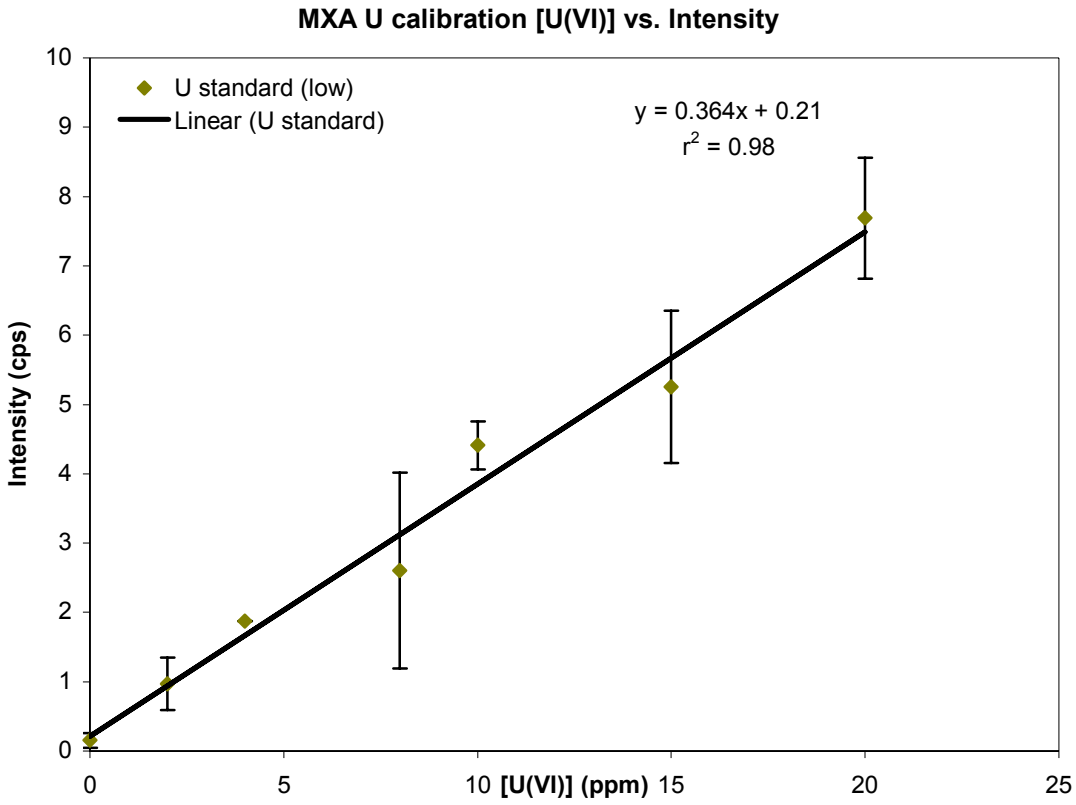


Figure 4-2. Calibration curve obtained for MXA analysis

It should be pointed out that the calibration curve does not go through the origin. The blank (5% nitric acid in nanopure water) sample showed some significant background intensity. This "blank" intensity is probably from the X-ray window film itself, nitric acid/nanopure water impurity, or some dust particles that were introduced during the sample preparation. Of those three, only the dust particle problem can be a localized effect. The acid/nanopure water impurity issue should affect all of the standard solutions in the series systematically, since the source of X-ray window films, nitric acid and the nanopure water is unique throughout. Moreover, the dust particle issue is the most difficult to control (if at all possible). Since the origin of the "blank" intensity cannot be specified or quantified, this "blank" intensity was left in the data (rather than subtracting the "blank" intensity from all subsequent data) for calibration.

**Sample Data**

After the calibration curve was constructed, the samples were measured, and then the concentrations were back-calculated based on the calibration curve. The results obtained from MXA and uranium analyzer methods were compared in terms of percent recovered, or a fraction of the "known" U concentration of the prepared samples recovered from MXA and UA-3 analyses. The concentration of the analyzed samples ranged from 0 to 500 ppm. Samples with concentrations higher than 20 ppm (beyond the calibrated range) were analyzed to: 1) decide whether the calibration curve (for 0 to 20 ppm) remains linear, and 2) observe the effect of increased U concentration upon error size. Figure 4-3 compares the two methods side by side. Again, the error bars represent the 95% confidence interval.

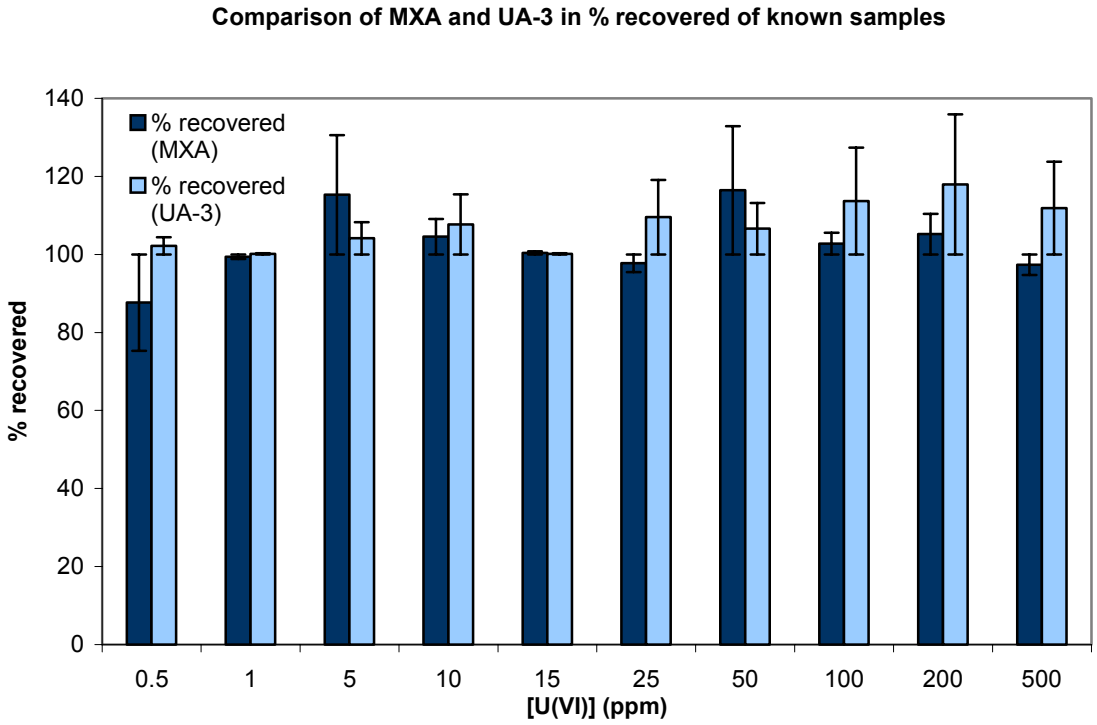


Figure 4-3 Comparison of MXA and UA-3 results in % recovered

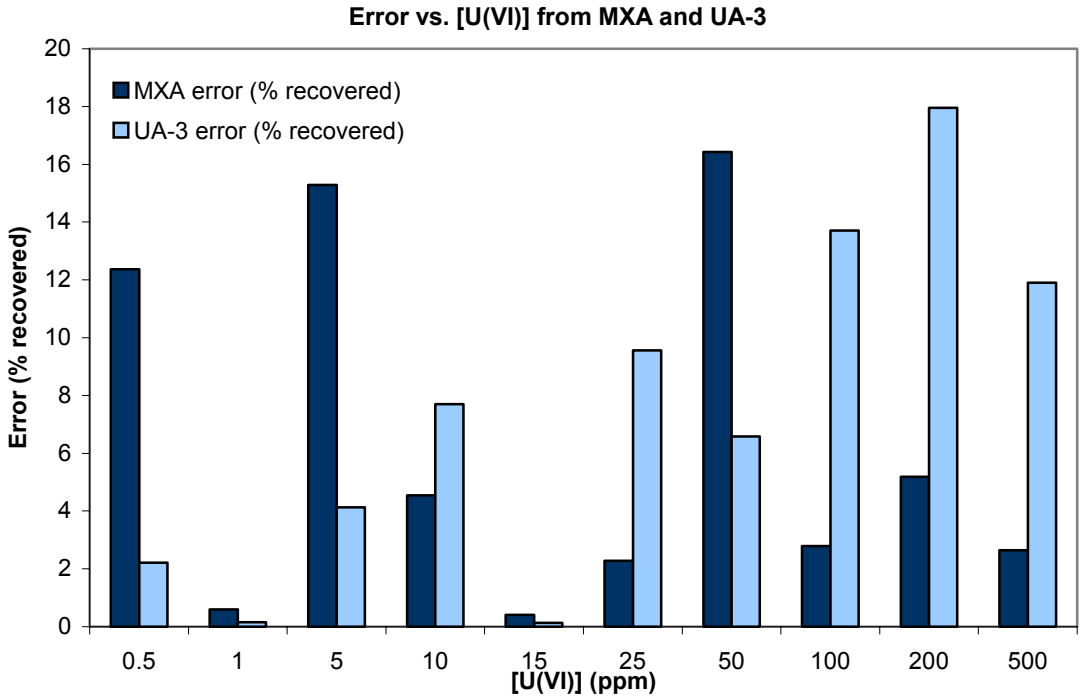


Figure 4-4. Error in % recovered from MXA and Uranium Analyzer

The percent recovery ranged from 88 to 116% for MXA-EDXRF method. UA-3 had recovered from 100 to 118%. To examine the error size with respect to U concentration, the error size in percent was compared between MXA-EDXRF and UA-3. Figure 4-4 provides a visual comparison of this.

The size of error from UA-3 increases for high U concentrations. This is due to the fact that, as the U concentration increases, the factor of dilution increases by orders of magnitude. Thus, the dilution error dominates the UA-3 error. By comparison, the error from the MXA-EDXRF method starts out large for lower concentrations (greater than 10%), and then declines to less than 5% from 10 ppm and upward (except for the 50 ppm-sample). The error size beyond 25ppm level was surprisingly small for the MXA-EDXRF data. This may be an indication that the calibration curve for U detection by MXA-EDXRF method may be linear for a large range, because the larger error size in lower concentration range may have come from the difficulty in obtaining data (probably too close to the detection limit).

The anomaly for the 50-ppm sample was probably due to the dust collection on the residue. Since the sample size is extremely small, all portion of the residue is probably seen by the incident X-ray. This also means that the matrix effect is minimal and the background is almost nonexistent. Therefore, when a foreign object (such as a dust particle) is present on the residue, it introduces heterogeneity to the specimen and possibly alters the true signal. It is even a possibility that, depending on the elemental composition of the dust particle, it can cause enhancement effect that the intensity of the signal becomes significantly larger than it should read from the analyte only.

Other MXA errors may be explained by three reasons: the positioning error, enhancement or absorption effect, and heterogeneous drying. If the residue looks as if the majority of the solid is on one side of the circular residue and almost none on the other side (or an appearance of a ring-like residue), it would give rise to matrix effect to a small degree. MXA errors at the high concentration end decreased, perhaps from the improved sensitivity of EDXRF at higher concentrations. For EDXRF, as seen before, the lowest detection limit is in the low ppm range.[1-5] The lower percentage of recovery at 0.5 ppm for MXA is in line with this. Based on near 100% recovery at 1 ppm, the realistic detection limit for the MXA-EDXRF method should be at around 1 ppm. Turner *et al.*[36] states that the minimum detection limit (MDL) can be approximated as

$$MDL = \frac{3 \cdot C\sqrt{Background}}{Peak \cdot \sqrt{t}} \tag{4-2}$$

where *Background* is the average background counts over the region of interest, *C* is the concentration of the standard in ppb, and *Peak* is the net peak counts over the region, and *t* being the measurement time. Based on this estimation, the MDL of the MXA samples hovers around 180 ppb for 1-ppm U standard solutions. However, with a thicker X-ray film and a heavier atom as the target element in this study, the lowest detection is around 1ppm U for accuracy.

Turner *et al.*[36] also suggests that acidification of the samples with low total dissolved solids (TDS) should aid in reducing the residue spot size. Low TDS samples generally contain less than 500 mg/L TDS. To test the effect of acidification on spot size, 5-ppm U standard solutions with different nitric acid content (0, 1, 5, and 10 vol%) were prepared, and analyzed by MXA-EDXRF method. As seen in the Figure 4-5, the result

did suggest that adding nitric acid to the sample reduces the spot size (decrease in spot size was noted from 0 to 1-% acid samples). However, no correlation was drawn from the obtained data.

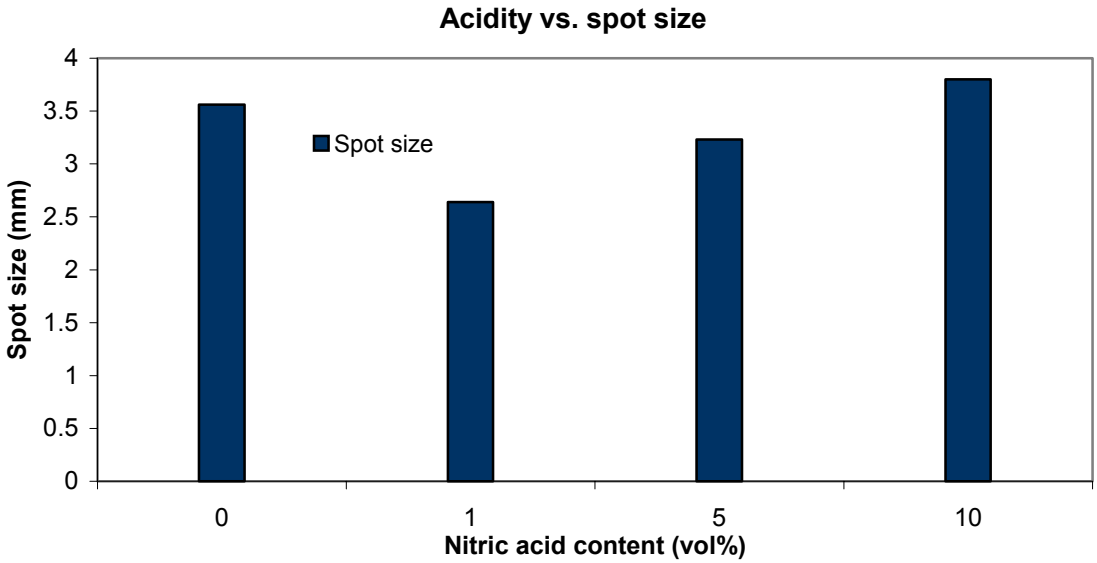


Figure 4-5. Nitric acid content and the spot size

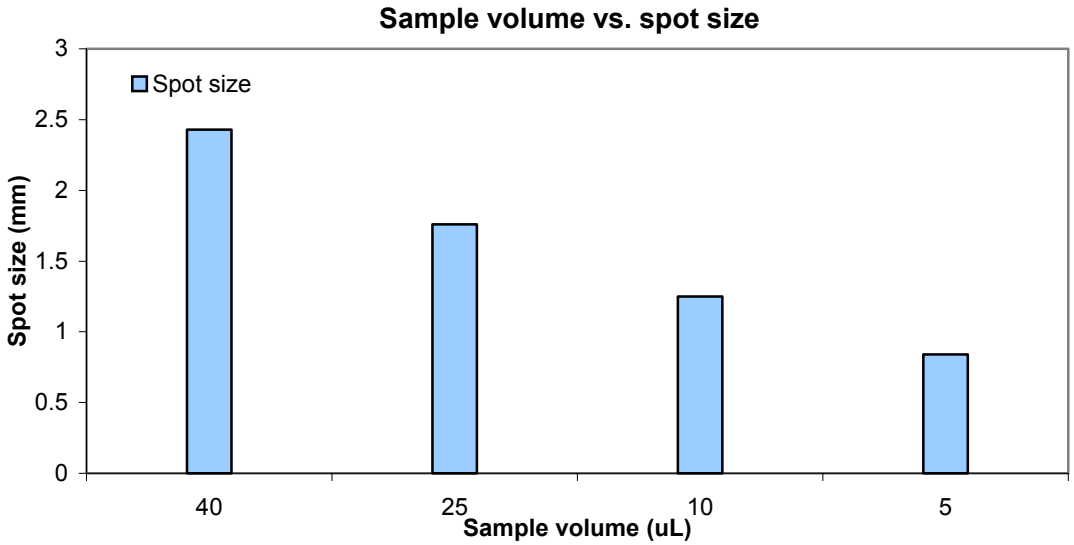


Figure 4-6. Sample volume vs. spot size

Another way to reduce the spot size, as suggested by Turner *et al.*,[36] is decreasing the sample volume loaded onto an X-ray film to dry. The suggested volume for sample

preparation is 50 μL, but it could be reduced to adjust the residue diameter to 2 to 3 mm. The effect of sample volume reduction was investigated. Figure 4-6 illustrates how the spot size decreases with decreasing sample volume. However, if the sample volume is changed, the entire calibration curve should be reconstructed for the newly chosen sample volume. Choosing a smaller sample volume may improve accuracy, since a smaller spot size makes the alignment of the residue to the X-ray beam spot easier. A smaller sample volume, on the other hand, increases the *MDL*.[36] Reducing the sample volume probably will not cause a major technical difficulty for U detection. This may not be a viable option for lighter elements, since the sample volume reduction leads to lower intensity. If the intensity is low to begin with, it will be even more difficult to detect such signals.

Another factor to consider is the U concentration. MXA spot size with respect to the U concentration was shown in Figure 4-7.

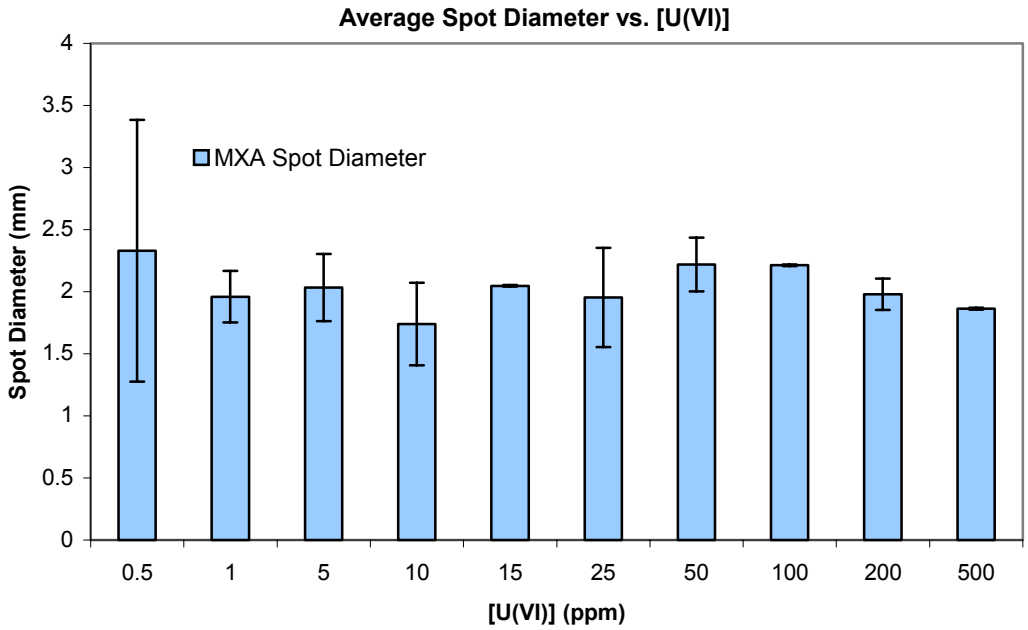


Figure 4-7. Spot size of analyzed samples

The error bars indicate the 95% confidence interval for the residue size. The most distinct result can be seen in 0.5-ppm U sample. On top of having the largest average spot size, the error size is much larger than others. This finding agrees with the claim that samples with lower TDS are more likely to suffer from the solid dissolved in the sample solution precipitating early on around the outer edge of the droplet.[36] This precipitation provides more sites for nucleation of remaining solids in the sample solution, which causes the residue to have a ring-like appearance. Even if the ring-like residue is smaller than the X-ray spot size, the sample can possibly suffer from the heterogeneity effect.

Finally, positioning error and the machine error were determined. To achieve this, 22 measurements were taken on the EDXRF for each of the three samples prepared for this experiment. The samples were all 35-ppm U standard solution samples prepared by MXA method. The spot size averaged at about 2 mm. The sample residues were aligned with the center spot of the sample holder for each measurement. Average U concentration was back-calculated (based on the calibration curve) for all three. The average [U(VI)] was found to be 40.5, 41.9, and 38.1 ppm U, respectively. The error sizes for each sample were 11.2, 11.4, and 10.8 %, respectively. Compared to Figure 4-4, it is obvious that the positioning/machine error is the dominant source of error. For samples 0.5, 5, and 50 ppm U, the error size ranged from 12 to 16% (from Figure 4-4). If the positioning/machine error (about 11% on the average) was subtracted from the total error for 0.5, 5, and 50ppm samples, the remaining error size (1 to 5%) corresponds with the total error exhibited by samples other than 0.5, 5, and 50 ppm. The samples other than those three had the total error size of from 0.5 to 5%. These results are in agreement with the error size for 0.5, 5, and 50 ppm U samples from sources other than the positioning error.

Therefore, it may be the case that samples other than 0.5, 5, and 50 ppm had almost no positioning error. The small error sizes for samples other than 0.5, 5, and 50 ppm U samples were most likely due to dust problems and minor matrix effects. It can be concluded that the accuracy for MXA measurements can be improved dramatically by aligning the residue to the beam spot with the utmost care.

After the method was researched and optimized, MXA sample preparation method was used to measure U concentrations in J-13 ground water. In the following, actual data from a urania-thoria powder dissolution experiment is presented.

**Application of MXA method – [U(VI)] measurement in ground water**

As a part of the NERI project 99-0153[7], a series of dissolution experiments were conducted. During one of the urania-thoria powder dissolution experiments, the MXA-EDXRF method was used to track the U concentration. The details of the study are given below.

The dissolution of $UO_2$ can be an enormously complex process, with a host of variables having a marked effect on the ultimate rate of corrosion. These variables can include solid properties, such as the O/M ratio, grain size, and grain boundary composition; and solution properties, such as pH, carbonate concentration, and the solution redox potential. This wide range of variables represents a particular challenge when comparing corrosion data obtained using different experimental conditions. A thorough definition of the experimental dissolution conditions is necessary in order to account for any variations that could result in significant differences in measured corrosion rates.

In this experimental work, the aqueous corrosion of $(U,Th)O_2$ has been investigated using powder samples. The high surface area of the powders will result in rapid

dissolution, and sampling intervals are closely spaced in the first several days of the experiments. For this study, J-13 ground water has been used as the leachate solution. The solutions are not replenished after each sample extraction in order to maintain a constant dissolved uranium concentration in equilibrium with the solid. This means that U(VI) saturation is probably reached in the solutions.

The dissolution experiments were performed over a six-week period in J-13 ground water. The $(U,Th)O_2$ powders used were synthesized using the oxalate precipitation method.[7] Nominal compositions of 5%, 20%, 35%, and 50% $UO_2$ were used, as well as a commercially supplied pure $UO_2$ powder. Powders prepared by the oxalate method were reduced at 800ºC for 10 h in Ar-5%H. Powder preparation and characterization was discussed elsewhere.[7]

The dissolution was carried out in 500 mL glass flasks, with 0.5 g quantities of powder added to 500 mL J-13 ground water (see Table 4-1).

Table 4-1. Composition of J-13 ground water [7]

| **Chemical species** | **Concentration (μg/mL)** |
|---|---|
| $Na^+$ | 45.8 |
| $K^+$ | 5.04 |
| $Mg^{2+}$ | 2.01 |
| $Ca^{2+}$ | 13.0 |
| $SiO_2$ | 61 |
| $HCO_3^-$ | 128.9 |
| $SO_4^{2-}$ | 18.4 |
| $Cl^-$ | 7.14 |
| $NO_3^-$ | 8.78 |
| $F^-$ | 2.18 |

The powder quickly settled to the bottom of the flasks. The flasks were fitted with rubber stoppers and air was bubbled through the solutions via glass pipets. The air bubbling acted to mix the solutions. Air flow was controlled for each vessel in the range of 10-15 mL/min using individual flow meters. The air was first humidified by bubbling through J-13 water in a gas washing bottle. Figure 4-8 shows the experimental dissolution setup. The experiments were carried out at room temperature, which was monitored throughout the duration of the experiment and was approximately 26ºC ±1ºC. Air was bubbled through a separate flask containing only 500 mL J-13 water in order to estimate the amount of solution evaporation over the duration of the experiments.[7]

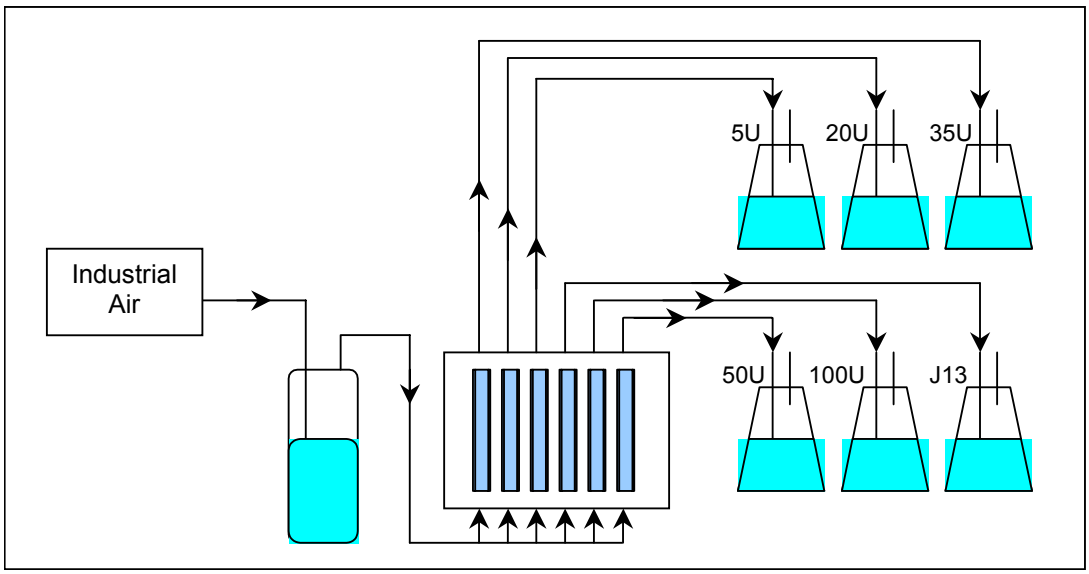


Figure 4-8. Schematic diagram of (U, Th)$O_2$ dissolution setup

Leachant samplings were performed at increasing time intervals over a total experiment duration of 1020 hours. A total of 17 samples were collected from each solution. Samples were extracted in 10 mL aliquots using a pipetter. The sample solutions were then passed through 0.02 μm filters and stored in glass vials prior to

analysis. The extracted volume was not replenished in order to maintain a constant concentration of dissolved species in the leachant. The calculation of the total amount of dissolved uranium takes into account the volume reduction from the extraction of consecutive samples.

Figure 4-9 shows the concentration of uranium in the leachant solution as a function of time over the first 92 hours of the experiment. In order to make meaningful comparisons between the different powders, the data was normalized with respect to both the available amount of uranium in the initial sample (determined by the sample mass and composition) and the surface area of the powder.[7] The normalized results are presented in Figure 4-10, which plots the fraction of the total initial uranium in the sample dissolved per $m^2$ surface area, $U_t/AU_i$, where $U_t$ is the mass of dissolved uranium after time t, A is the powder surface area, and $U_i$ is the initial mass of uranium in the sample. This eliminates the surface area and sample composition as variables, and allows direct comparison between the dissolution rates for different powders.

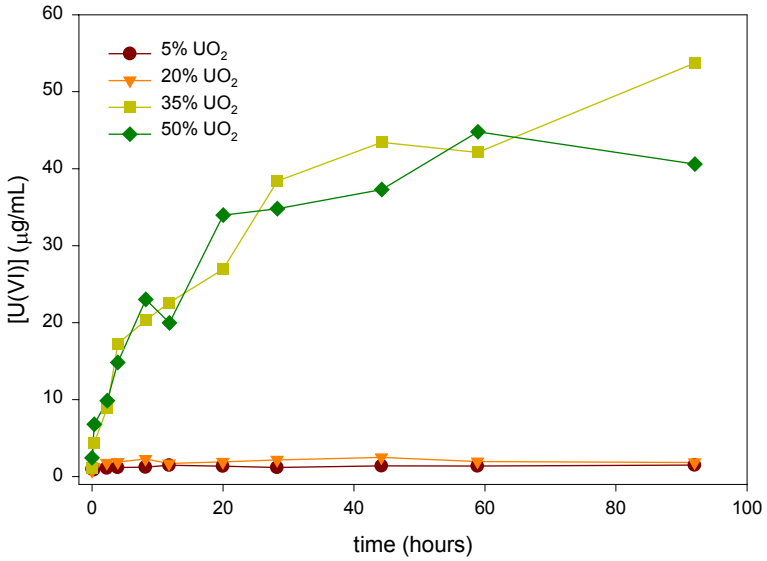


Figure 4-9. Concentration of uranium measured in the leachate solutions as a function of dissolution time

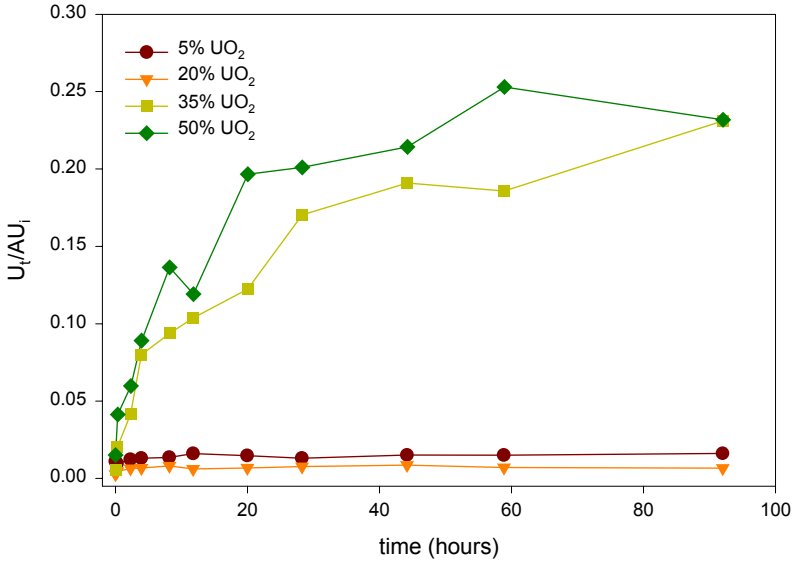


Figure 4-10. Fraction of total uranium dissolved per $m^2$ powder surface area

A number of important observations can be made on the preliminary data in Figure 4-10. Both the 5% and 20% $UO_2$ powders exhibited relatively low dissolution rates. In contrast, the 35% and 50% $UO_2$ powders exhibited dissolution rates significantly larger after 124 hours. This indicates a significant difference in dissolution behavior between these two ranges of powder composition, a result that has clear implications for the storage of spent fuels.

As presented above, the MXA method proved to be a viable means to measure the concentration of U in J-13 ground water quantitatively.

## Conclusion

Quantitative determination of trace U in water by microsample X-ray analysis (MXA) sample preparation method, followed by the EDXRF analysis, was investigated in this study. The method has many advantages. The MXA sample preparation method offers a much higher sample turnout compared to other characterization methods available. The XRF analysis is one of the most rapid means of spectrometry, and the

MXA sample preparation procedure takes only about 5 minutes. The method is very inexpensive. Only supplies (besides reagents) needed for sample preparation are XRF sample cups, X-ray window films, and some micropipetters of appropriate volume settings. The simplicity of the MXA sample preparation method may allow application and adaptation for other target elements. The amount of radioactive waste water generated from the MXA sample preparation procedure is minimal, which is extremely favorable in terms of environmental protection. From a scientific standpoint, it is always beneficial to have as many methods as possible for a single characterization purpose. If more methods are available, one will be able to: choose from a list of methods based on needs and the resource readily available, and will have more opportunities for data verification.

Some adaptation (to suit the needs for different target elements) include acidification of samples for spot size control for dilute samples, switching the X-ray film to a thinner kind (especially for lighter elements and an improved transmission of signals[36]), sample volume reduction, and the XRF parameter adjustments. This method is easy to follow and it requires a minimal amount of instruction. As long as the samples used for calibration and the real samples have the matrices similar to each other, matrix effects are minimized. Minimizing the matrix effects improves data accuracy.

Applications of this method include the tracking of U leaching behavior in a simulated ground water storage condition and the analysis of surface water samples. In conjunction with other characterization methods such as ICP-MS, ICP-AES, ICP-OES, CVAA, GFAA, and uranium analyzer, the MXA sample preparation method, followed by

the XRF analysis, can provide an affordable, quick, and simple alternative to materials characterization.

LIST OF REFERENCES


1. R. Jenkins, X-Ray Fluorescence Spectrometry, Second Edition, Wiley and Sons, New York, 1999.

2. E. Bertin, Principles and Practice of X-Ray Spectrometric Analysis, Second Edition, Plenum Press, New York, 1975.

3. T. Dzubay (Ed), X-Ray Fluorescence Analysis of Environmental Samples, Ann Arbor Science, Ann Arbor, 1977.

4. G. Lachance, F. Claisse, Quantitative X-Ray Fluorescence Analysis: Theory and Application, Wiley and Sons, New York, 1995.

5. H. Bennett, G. Oliver, XRF Analysis of Ceramics, Minerals and Allied Materials, Wiley and Sons, New York, 1992.

6. V. Buhrke, R. Jenkins, D. Smith (Ed), A Practical Guide for the Preparation of Specimens for X-Ray Fluorescence and X-Ray Diffraction Analysis, Wiley and Sons, New York, 1998.

7. Nuclear Engineering Research Initiative (NERI) project #99-0153 Advanced Proliferation Resistant, Lower Cost Uranium-Thorium Dioxide Fuels for Light Water Reactors, Second Annual Report (INEEL/EXT-01-00804) 2001.

8. L.M. Bernardo, R.B. Clark, D. Knudsen, J.W. Maranville, Comm. Soil Sci. Plant Anal. 16 (8) (1985) 823.

9. R.E. Van Grieken, C.M. Bresseleers, B.M. Vanderborght, Anal. Chem. 49 (9) (1977) 1326.

10. P. Minkkinen, Finn. Chem. Lett. 4-5 (1977) 134.

11. P.J. Potts, A.T. Ellis, P. Kregsamer, C. Streli, M. West, P. Wobrauschek, J. Anal. At. Spectrom. 14 (1999) 1773.

12. P.J. Potts, A.T. Ellis, P. Kregsamer, J. Marshall, C. Streli, M. West, P. Wobrauschek, J. Anal. At. Spectrom. 16 (2001) 1217.

13. M.R. Cave, O. Butler, S.R.N. Chenery, J.M. Cook, M.S. Cresser, D.L. Miles, J. Anal. At. Spectrom. 16 (2001) 194.

14. R. Hoelzl, L. Fabry,.L. Kotz, S. Pahlke, Fresenius J. Anal. Chem. 366 (2000) 64.

15. D. Darbouret, I. Kano, J. Anal. At.Spectrom.15 (2000) 1395.

16. R. Sutarno, H. F. Steger, Talanta 32 (6) (1985) 439.

17. C. Reimann, U. Siewers, H. Skarphagen, D. Banks, Sci. Total Environ.239 (1999) 111.

18. C. Reimann, U. Siewers., H. Skarphagen, D. Banks, Sci. Total Environ.234 (1999) 155.

19. T.H. Nguyen, J. Boman, M. Leermakers, W. Baeyens, X-ray Spectrometry 27(4) (1998) 277.

20. S. Kurunczi, S. Torok, J.W. Beal, X-ray Spectrometry 28(5) (1999) 352.

21. Kallithrakas-Kontons, K. Zoumi, S. Nikolakaki, P. Kritidis, J.Radioanal. Nucl. Chem. 227(1-2) (1998) 61.

22. H. Cadle, P. A. Mulawa, E. C. Hunsanger, K. Nelson, R. A. Ragazzi, R. Barrett, G. L. Gallagher, D. R. Lawson, K. T. Knapp, R. Snow, Environ. Sci. Technol. 33(14) (1999) 2328.

23. T. S. Aisueva, T. N. Gunicheva, J. Anal. Chem.54 (11) (1999) 1085.

24. A. Mendoza, R. C., M. Valdes, J. J. Meitin, R. Perez, Y. Lorente, J. Radioanal. Nucl. Chem. 240 (2) (1999) 459.

25. K. Katahira, M. Y., S. Morisawa, Environ. Technol. 21 (5) (2000) 505.

26. I. Szaloki, A. Somogyi, M, Braun, A. Toth, X-ray Spectrom. 28 (5) (1999) 399.

27. C.U. Ro, S. Hoornaert, R. Van Grieken, Anal. Chim. Acta 389 (1999) 151.

28. I.E. De Vito, A.N. Masi, R.A. Olsina, Talanta 49 (1999) 929.

29. S. Latva, S. Peraniemi, Markku Ahlgren, Analyst 124 (1999) 1105.

30. A.N. Masi, R.A. Olsina, J. Trace Microprobe T. 17(3) (1999) 315.

31. Y.N. Makarovskaya, L. P. Eksperiandova, A.B. Blank, J. Anal. Chem. 54 (11) (1999) 1031.

32. M.E. McComb, H.D. Gesser, Talanta 49 (1999) 869.

33. R.A. Dewberry, Nucl. Instrum. Meth. A 403 (1998) 383.

34. M.S. Carvalho, M.L.F. Domingues, J.L. Mantovano, E.Q.S. Filho, Spetrochim. Acta B 53 (1998) 1945.

35. M.S. Carvalho, J.A. Medeiros, A.W. Nobrega, J.L. Mantovano, V.P.A. Rocha, Talanta 42 (1) (1995) 45.

36. D.C. Turner, M. Benson, A. Wilson, J. Moore, W. Watson, Am. Lab. 32 (2000) 92.

37. Philips Analytical B. V., Philips Analytical MiniPal PW 4025 User's Guide, Second Edition, Philips Eletronics N. V., Almelo (The Netherlands), 1999.

38. Scintrex Limited, UA-3 Uranium Analyzer Operators Instiructions, Scinterx Limited, Concord (Canada), 1983.

## BIOGRAPHICAL SKETCH

Noriko Shibuya was born on October 28, 1973. She received her Bachelor of Science in Chemical Engineering and Bachelor of Science in Electrical Engineering degrees from Northwestern University in Evanston, IL. She went on to pursue her Master of Science degree at the University of Florida under Dr. Ronald H. Baney, in the Department of Materials Science and Engineering.